One gene - two proteins: The C-terminus of the prototypical M2 muscarinic receptor localizes to the mitochondria

Irene Fasciani[a†], Francesco Petragnano[a†], Ziming Wang[b], Ruairidh Edwards[c], Narasimha Telegu[b], Ilaria Pietrantoni[a], Henrik Zauber[b], Mario Rossi[c], Ulrike Zabel[d], Marlies Grieben[b], Maria Eirini Terzenidou[c], Jacopo Di Gregorio[a], Cristina Pellegrini[a], Silvano Santini Jr[e], Anna Rita Taddei[f], Barbel Pöhl[b], Stefano Aringhieri[g], Gabriella Aloisi[a], Francesco Marampon[h], Alexandra Roman[b], Sebastian Diecke[b], Vincenzo Flati[a], Franco Giorgi[f], Fernanda Amicarelli[e], Andrew B. Tobin[c], Marco Scarselli[g], Kostas Tokatlidis[c], Martin J Lohse[b,d,i]*, Roberto Maggio[a]*, Paolo Annibale[b]*

[a] Department of Biotechnological and Applied Clinical Sciences, University of L'Aquila, 67100 L'Aquila, Italy.
[b]Max Delbrück Center for Molecular Medicine, 13125 Berlin, Germany.
[c]Centre for Translational Pharmacology, Institute of Molecular, Cell and Systems Biology, College of Medical, Veterinary and Life Sciences, University of Glasgow, G128QQ Glasgow, UK.
[d]Institute of Pharmacology and Toxicology, University of Würzburg, 97078 Würzburg, Germany.
[e]Department of Life, Health and Environmental Sciences, University of L'Aquila, 67100 L'Aquila, Italy.
[f]Section of Electron Microscopy, Great Equipment Center, University of Tuscia, Viterbo, Italy.
[g]Department of Translational Research and New Technology in Medicine, University of Pisa, 56126 Pisa, Italy.
[h]Department of Radiotherapy, University of Roma La Sapienza, 00151 Roma, Italy
[i]ISAR Bioscience Institute, 82152 Munich, Germany
[†] equal contribution

*email: m.lohse@mdc-berlin.de;

*email: roberto.maggio@univaq.it;

*email: paolo.annibale@mdc-berlin.de

31 **Abstract**

32 **Muscarinic acetylcholine receptors are G protein-coupled receptors (GPCRs) activated by the**
33 **endogenous neurotransmitter acetylcholine. We show here that the carboxyl terminal fragment of the**
34 **muscarinic M_2 receptor, containing the transmembrane regions 6 and 7 (M_2tail), is expressed by virtue**
35 **of an internal ribosome entry site. Radioligand binding, biochemical and molecular biology experiments,**
36 **combined to advanced fluorescence microscopy reveal that the M_2tail, whose expression is upregulated**
37 **in cells undergoing integrated stress response, does not follow the normal route to the plasma membrane,**
38 **but is almost exclusively sorted to the mitochondria inner membrane: here it controls oxygen**
39 **consumption, cell proliferation and the formation of reactive oxygen species via reduction of oxidative**
40 **phosphorylation. Genetic editing of the key methionine where cap-independent translation occurs,**
41 **reveals the physiological role of this process in influencing cell proliferation and oxygen consumption.**
42 **The expression of the carboxyl-terminal of a GPCR, capable of regulating mitochondrial function,**
43 **constitutes a hitherto unknown mechanism that cells may use for controlling their metabolism under**
44 **variable environmental conditions, notably unrelated to the canonical signalling function of the GPCR**
45 **at the plasma membrane.**

46

47 Muscarinic receptors include five structurally related receptors, belonging to class A of the G protein-coupled
48 receptor (GPCR) family[1]. They are comprised of seven trans-membrane domains (TM domains 1-7) connected
49 by intra and extracellular loops. Of these structural elements, the third intracellular (i3) domain is the one
50 conferring a coupling specificity for G proteins, β-arrestin recruitment and endocytic internalization [2].
51 However, only a small portion of the i3 loop is required for receptor function, and for this reason large deletions
52 of this segment have no effect on receptor activation and internalization [3].

53

54 We could previously show that the M_2 receptor can be split at the level of the i3 loop into two segments, each
55 behaving as an autonomous folding unit capable of targeting the plasma membrane and surprisingly
56 reconstituting a physiologically active receptor when expressed together in transfected cells [4]. In the context
57 of these studies, a mutant of the receptor carrying a stop codon in position 228 was surprisingly observed to
58 retain (albeit reduced) ligand binding in radioligand binding assays [11]. This finding cannot be explained by the

59 fact that the insertion of the stop codon results in the expression of an N-terminal receptor fragment, constituted
60 by the TM regions 1-5, since this fragment alone has been shown to be not able to bind muscarinic ligands and
61 to trigger signal transduction [12]. Therefore, an alternative explanation for the behavior of stop-codon mutant
62 228 is needed. Since the N-terminal fragment can reconstitute a physiologically active receptor when co-
63 transfected with the C-terminal fragment, a plausible possibility is that the C-terminal segment of the receptor
64 can be independently produced and reconstitute an active receptor with the N-terminal portion on the cell
65 membrane. This scenario opens the interesting question of how the C-terminal fragment can be translated
66 endogenously as an independent polypeptide.
67
68 In eukaryotes, the most common mechanism of translation initiation is the cap-dependent process, which
69 requires the interaction of several key proteins at the 5'-end (5′ cap) of mRNA molecules. However, in recent
70 years, it has been demonstrated that the presence of internal ribosome entry site (IRES) sequences, which are
71 common features of virus replication[5], can mediate cap independent translation of eukaryotic RNA(s) [6]. This
72 presents the suggestive possibility that a cap-independent translation of the M_2 C-terminal domain indeed
73 occurs in this mutant, opening a number of important questions about the molecular processes involved in the
74 synthesis and subcellular behaviour of the C-terminal domain fragment.
75
76 GPCRs are normally distributed at the plasma membrane, where, after activation by an agonist and coupling
77 to G proteins, regulate a number of intracellular effectors. Nevertheless, non-canonical localizations of GPCRs
78 have also been described, such as in endosomes [7], cell division compartments (centrosomes, spindle midzone
79 and midbodies)[8], and mitochondria [9 10], underpinning non-traditional roles for this protein family.
80
81 In this work, we therefore set out to explore whether the expression of the C-terminal domain of the M_2
82 muscarinic receptor, a region containing the TM regions 6 and 7, occurs naturally by a cap-independent
83 translation mechanism. Combining radio-ligand binding, molecular biology approaches, advanced
84 fluorescence imaging and genetic editing of human induced pluripotent stem cells (hiPSCs) we have observed
85 that the C-terminal domain of this receptor is indeed expressed as an independent polypeptide. Surprisingly,
86 using bimolecular fluorescence complementation, in-vitro mitochondrial import assays and cell metabolism

87 assays we observe that the C-terminal domain is strongly targeted to the cell mitochondria. Importantly, this
88 mitochondrial targeting has functional ramifications since both cap-dependent mediated overexpression of the
89 C-terminal domain alone, as well as cap-independent mediated translation starting from the mRNA of the full
90 length M_2 receptor, resulted in a sizable reduction of oxidative phosphorylation.
91 In summary, our study reports the new observation that alternative reading of a GPCR receptor gene can
92 translate into a fragment of the receptor that serves a cellular function entirely different from canonical GPCR
93 signalling.
94
95 **Results**
96 **Ligand binding and functional properties of M_2 receptors mutants**.

97 To investigate and distinguish the functional roles of the two known N-terminal (TM1-5) and C-terminal
98 (TM6-7) domains of the M_2 muscarinic receptor, we expressed C-terminally truncated variants of the receptor
99 in COS-7 cells. We first observed that the M_2stop228 construct, a receptor mutant bearing a stop codon at the
100 beginning of the i3 loop in position 228 (but containing the downstream sequence, i.e. leading to the
101 transcription of an mRNA of the same length as that of the wt M_2R) (**Fig. 1a** and **Supplementary Fig. 1**),
102 exhibited unexpected binding activity [11] albeit at a very low level of expression, i.e. 45 fmol/mg of protein.
103 Both K_D value of [^{3}H]NMS (N-methylscopolamine, an antagonist) calculated from direct saturation
104 experiments, and the IC_{50} values, calculated in competition experiments for the agonist carbachol, were in fact
105 similar to those calculated for the wild type M_2 receptor (**Table 1**). Furthermore, the M_2stop228 receptor was
106 found functionally active as it was capable to inhibit adenylyl cyclase [11] and increase ERK phosphorylation
107 (**Supplementary Fig. 2b**), even though the extent of response was reduced if compared to the wild type M_2
108 receptor. On the other hand, if a stop codon is inserted upstream or downstream of position 228, e.g. at positions
109 196 or 400, no radioligand binding can be observed (**Fig. 1a** and **Supplementary Table 1**).

110 As we demonstrated in an earlier report [12], another receptor fragment whose sequence runs only until position
111 283 (i.e. comprising only TM1-5) of the corresponding wt receptor, called M_2trunk(1-283) (**Supplementary**
112 **Fig. 1**), did not show any radio-ligand binding activity upon expression in COS-7 cells, despite comprising the
113 first five trans-membrane regions of the wild type M_2 receptor, as the M_2stop228 construct (**Table 1**).

114 Consistently, a construct containing only the M_2 receptor sequence until amino acid 228 (M_2trunk(1-228)), did
115 not show any radio-ligand binding (**Table 1**).

116 On the other hand, we observed binding and downstream signaling ability in co-transfection experiments of
117 the M_2trunk(1-283) and M_2tail(281-466) (**Table 1**), the latter being a construct containing only the sequence
118 between aminoacid 368 and the end of the M_2 receptor, i.e. comprising TM6 and 7. Therefore, co-expression
119 of the M_2trunk(1-283) (TM1-5) and M_2tail(368-466) (TM6-7) reconstitutes a functional full length receptor at
120 the cell membrane (**Fig. 1b**).

121 These data suggest that, for the M_2stop228 receptor to display binding and functional activity, the receptor
122 sequence downstream of the stop codon in position 228 (containing TM6 and 7) has (i) to be translated and
123 (ii) to presumably interact with the first five TM regions of the M_2 receptor. This notion is graphically
124 summarized in **Fig. 1b.** For this hypothesis to be true, however, the C-terminal portion of the receptor needs
125 to be expressed despite the presence of stop codons in the i3 loop in our M_2stop228 mutant. Indeed, we
126 confirmed expression of the C-terminal fragment by fusing an enhanced Green Fluorescent Protein (EGFP) at
127 the C terminus of several receptor mutants (**Fig. 1c).**

128 Interestingly, though, while cells expressing the M_2-EGFP displayed the normal, predominant plasma
129 membrane expression (**Fig. 1c**), cells expressing the M_2stop228-EGFP displayed a visible intracellular green
130 fluorescence, which is in stark contrast to cells expressing M_2stop400-EGFP, which do not show any
131 fluorescence, in line with the non-transfected control.

132 To further analyze the atypical behavior of M_2stop228-EGFP, which by displaying green fluorescence
133 confirms that the sequence downstream of the stop in position 228 is indeed translated, we generated a frame
134 shift mutant: we inserted a single guanine nucleotide in the sequence of the M_2-EGFP, changing the methionine
135 in position 368 into an aspartate, which in turn generates an in-frame stop codon at position 370. We named
136 the construct, which notably still displays an EGFP signal in transfected cells, M_2fr.sh.-EGFP (**Fig. 1c**). The
137 observation that the mutant retains EGFP fluorescence is most remarkable, since the EGFP is now out of the
138 original reading frame and it can only be properly translated by a cap-independent translation mechanism,
139 starting from a methionine in the new reading frame.

140 Furthermore, the observation that both M_2stop228-EGFP and M_2fr.sh.-EGFP retain EGFP fluorescence,
141 whereas M_2stop400-EGFP does not, indicates not only that a cap independent translation mechanism occurs,
142 but also that the starting methionine for the process must be downstream of stop 228 and upstream of stop 400,
143 leaving as a leading candidate the third in-frame methionine of the i3 loop. This is in line with the radio-ligand
144 binding data from co-expression of receptor mutants carrying a double stop codon, the first in position 228 and
145 the second in positions ranging from 248 to 400, including mutations of the first (M248) and second (M296)
146 in-frame methionines in the third i3 loop (**Supplementary Table 1, Fig. 1a** and **Supplementary Fig. 2a)**,
147 further pointing to M368 as the most likely site for the cap-independent initiation of translation of the C-
148 terminal domain.

149

150 **Immunodetection of the M_2 carboxyl terminal fragment**

151 To further characterize the expression of the C-terminal fragment and verify the hypothesis of cap-independent
152 translation, we tagged several of the M_2 receptors mutants described above with a myc-tag for immune
153 detection. The constructs were subcloned in a bicistronic vector backbone, allowing also the expression of the
154 red fluorescent protein mRuby2 as a fluorescent reporter, in order to verify comparable expression levels.
155 HEK293 cells were therefore transfected with the wild type M_2 receptor M_2-myc, the C-terminal fragment
156 starting at the third in-frame methionine M_2tail(368-466)-myc, a mutant of the M_2 receptor with the third in-
157 frame methionine mutated to an alanine, M_2M368A-myc that as discussed above should affect the cap-
158 independent translation, and finally the M_2stop400-myc; the constructs were resolved by SDS-PAGE and
159 assayed by Western blotting, as displayed in **Fig. 2a**. Based on the amino acid sequence, the expected molecular
160 weights for the full length receptor and the C-terminal fragment (inclusive of the myc tag) are ~75 kDa and
161 ~13 kDa respectively.

162 Interestingly, M_2tail(368-466) runs with two clear bands ~20 and ~15 kDa (**Fig. 2a**), indicating the presence
163 of post-translational modifications and protein processing (see **Discussion)** and thus defining the qualitative
164 pattern expected for the M_2 carboxyl terminal fragment starting at the third in-frame start codon (M368). The
165 full-length receptor was observed, as expected, at about ~75 kDa together with commonly observed higher
166 order oligomers[13]. Notably, the M_2 receptor clearly displays the lower MW band pair also seen for M_2tail(368-
167 466). The strongest confirmation for a cap-independent translation process is found in the M_2M368A: here the

168 ~20 kDa band disappears. In line with what we observed for its EGFP tagged version, the M_2stop400 does not
169 exhibit any band, comparable to the negative control using untransfected cells. The absence of any band further
170 excludes the possibility of a downstream cap-independent translation site yielding a fragment originating from
171 the next in frame methionine (406) (**Fig. 2a**). Altogether these results support the notion that the band at ~20
172 kDa observed in the wild type M_2 receptor lane is the bona-fide tail fragment originated by a cap-independent
173 translation mechanism, and that the origin of this process is at the third in frame methionine (M368) of the M_2
174 receptor.
175 We then tested whether a similar phenomenon, namely the translation of the C-terminal portion of the M_2
176 receptor, could be observed endogenously in physiological settings. We therefore prepared protein extracts
177 from heart, brain and spleen tissues from a line of knock-in mice (see **Methods**), designed to have expression
178 of a Chrm2/tdtomato fusion protein driven by the endogenous M_2 muscarinic acetylcholine receptor
179 promoter/enhancer sequences. The heart and brain are known to express sizable levels of the M_2 receptor,
180 whereas the spleen, where no expression of the M_2 receptor is reported in the proteomic databases, was used
181 as a negative control.
182 The use of a transgene tag was necessary, since antibody against the M_2 receptor are notoriously ineffective,
183 in particular when targeted at the C-terminal portion of the receptor. Instead, the tdtomato fluorescent protein
184 can be targeted by a specific polyclonal antibody, as shown by the Western blot displayed in **Fig. 2b**. As
185 expected, the full-length receptor-tdtomato fusion was observed at ~130 kDa (~75 kDa contributed by the
186 receptor and ~55 kDa contributed by tdtomato).
187 Notably, both in the heart and brain, but not in the spleen, of these knock-in animals we observed a band
188 doublet at ~75 kDa, which corresponds to the sum of the molecular weights of the tail fragment (~20 kDa, see
189 above and **Fig. 2a**) and the molecular weight of tdtomato.
190
191 **Testing bicistronic constructs for the presence of an IRES**.
192 To explain the translation of the carboxyl terminal fragment of the M_2 receptor, a mechanism enabling a cap-
193 independent initiation of protein synthesis should be hypothesized [5,6]. Accordingly, an IRES should be found
194 downstream of the artificial stop codon 228 and upstream of the third in-frame methionine (codon 368) of the
195 i3 loop. Before testing this hypothesis, we first ruled out several alternative mechanisms that could lead to the

196 translation of M2tail, such as stop codon read-through, termination-reinitiation and alternative splicing in the
197 translation of M2tail, as discussed in the **Supplementary Information** and in **Supplementary Figure 3**).
198 Then, to test the hypothesis that an IRES is leading to the cap-independent translation of the C-terminal domain,
199 we prepared a fluorescence reporter construct in which the i3 loop of M_2 (from nucleotide 685 (a.a. 228) to
200 nucleotide 1101 (a.a. 368)) was inserted between the two fluorescent proteins Sirius and EGFP (**Fig. 3a**). This
201 construct, named Sirius-M_2i3(417n)-EGFP, would translate Sirius according to the classical cap-dependent
202 mechanism, and, at the same time, it would drive EGFP translation only if the M_2i3 loop contains an IRES
203 sequence, effectively acting as a bicistronic expression cassette. We transfected several cell lines with this
204 construct, all positive for the blue and green fluorescence **(Supplementary Fig. 4)**. HEK293, used throughout
205 our study, also appeared positive for both the blue and green fluorescence, as shown in the inset of **Fig. 3a**.
206 To rule out the possibility that EGFP translation from the Sirius-M_2i3(417n)-EGFP construct could be due to
207 read-through and termination-re-initiation mechanisms, a mRNA hairpin loop was inserted in the sequence
208 after the stop codon of the Sirius protein. The resulting construct (named Sirius-H-M_2i3(417n)-EGFP) showed
209 only a slight reduction of the EGFP/Sirius with respect to the value measured for the analogous reporter without
210 hairpin (~90%) (**Fig. 3a**). In contrast the Sirius-H-EGFP plasmid, where the entire M_2i3 loop after the Sirius
211 was removed, showed a negligible EGFP/Sirius ratio (below 5%), underlining the importance of the i3 loop
212 for EGFP expression (**Fig. 3a**). Notably, when the hairpin was inserted within the i3 loop of the full length M_2-
213 EGFP, upstream of the M368, it was still possible to observe GFP fluorescence (**Supplementary Fig. 5)**.
214 To narrow down the position of the IRES sequence we divided the M_2 i3 loop in three parts and the resulting
215 nucleotide sequences, 685-699, 685-1071 and 685-699/1072-1101, were inserted downstream of the hairpin
216 loop in three different constructs (**Fig. 3a** and **Supplementary Fig. 6)**.
217 EGFP fluorescence was not significantly rescued upon insertion of the first 15 nucleotides (685-699) of the i3
218 loop after the hairpin, nor by the addition of the subsequent 372 nucleotides (685-1071). However, when the
219 last portion of the M_2 i3 loop was inserted in the construct after the Hairpin, leading to Sirius-H-M_2i3(15n/30n)-
220 EGFP, ~110 % of the value measured for the Sirius-M_2i3(417n)-EGFP plasmid was recovered (**Fig. 3a**).
221 These results strongly suggest that the IRES is located in a region of the i3 loop sequence immediately upstream
222 of the third methionine (M368) (see **Fig. 1a**), as also confirmed from ribosome profiling data from human left
223 ventricle tissue, displaying increased p-sites as well as overall ribosomal coverage in correspondence of this

224 region. This conclusion is further supported by the finding that when each of the three in-frame i3loop
225 methionines (namely M248, M296 and M368) after the stop codon 228 of the M_2stop228 were mutated to an
226 additional stop codon, only the mutation of M368 to a stop codon proved capable of completely abolishing
227 [^{3}H]NMS binding (**Supplementary results** and **Supplementary Fig. 1 and Supplementary Table 1**). These
228 binding results can furthermore rule out read-through and termination re-initiation: if these mechanisms were
229 responsible for translation of the C-terminal of the M_2stop228, suppression of the first methionine would have
230 abolished the binding. Finally, the origin of the carboxyl terminal fragment of M_2 at the third in-frame
231 methionine (M368) is also supported by the key observation that the mutant M_2-M368A does not display the
232 ~20 kDa band for the M_2 C-terminal fragment as compared to the wild type M_2 receptor in the Western blot of
233 **Fig. 2a**.
234
235 Based on this evidence, we mutated the conserved residues highlighted in yellow in **Supplementary Fig. 6a**,
236 in order to check for their relevance in recruiting the ribosome on the M_2 i3 loop sequence, as shown in **Fig.**
237 **3b**. As discussed in detail in the **Supplementary Results**, we found that the four nucleotides AAGA1090-
238 1093 next to the methionine 368 play a pivotal role in recruiting the ribosome on the M_2 mRNA and in
239 translating the M_2 C-terminal fragment.
240
241 **Generalization to other members of the GPCR superfamily**
242 In order to determine if the observed behavior is specific to the M_2 receptor, or could highlight a feature
243 common to other members of the GPCR superfamily, we repeated several of our experiments in another GPCR,
244 the related muscarinic M_3 receptor. The M_3 displays an in-frame methionine at the end of the i3loop, in position
245 481 (**Supplementary Fig. 6a)**. We then inserted a stop codon in position 273, generating the construct
246 M_3stop273 that still displayed radio-ligand binding. Several other mutants, mimicking the single and double
247 stop mutations performed for the M_2 displayed a behavior consistent with M481 being the start point of a cap-
248 independent translation of the C-terminal also for the M_3 receptor (**Supplementary Tables 2 and 3)**, thus
249 indicating that IRES-mediated cap-independent translation of the C-terminal domain could be a phenomenon
250 not restricted solely to the M_2 receptor, but may be shared at least by some other members of the GPCR
251 superfamily. The presence of an IRES sequence upstream of M481 further appears to be supported by the

252 observation that 558 nucleotides from the i3 loop of the M_3 receptor (from nucleotide 880 to 1437) were
253 inserted in the same Sirius-EGFP reporter construct as used for the M_2 (**Supplementary Fig. 6b**). This appears
254 to be indeed supported by the sequence-alignment of the five muscarinic receptors. The alignment of the last
255 portion of the M_2 i3 loop (from nucleotide 1072 to 1104) with regions adjacent to the second (M_1), fourth (M_3
256 and M_4) and first (M_5) in-frame Methionines, clearly shows that some nucleotide residues are conserved
257 (**Supplementary Fig. 6a)**. Overall these data underline that cap-independent translation could be a more
258 general feature of GPCRs mRNAs.
259

260 **Localization of the M_2 C-terminal fragment generated by cap-dependent expression under the control**
261 **of a viral promoter**

262 After having established that the expression of the M_2 C-terminal domain is regulated by an IRES and that its
263 translation starts at M368, we went on to study the role it might play in the cell. For this purpose, M_2tail(368-
264 466) fused to the fluorescent protein EGFP in pcDNA3, that is under the control of a strong CMV promoter,
265 was expressed in HEK293 cells in order to study the subcellular localization of this domain. Confocal
266 microscopy demonstrated a striking mitochondrial localization of the M_2tail(368-466)-EGFP construct (**Fig.**
267 **4a**). We confirmed this observation by co-staining HEK293 cells with a conventional mitochondrial stain
268 (Mitotracker Deep Red) and by co-expressing M_2tail(368-466)-EGFP with Tom20-mCherry, a fluorescently
269 labeled construct targeted to the outer mitochondrial membrane (**Supplementary Fig. 7a**). The observed
270 mitochondrial localization of the M_2tail(368-466)-EGFP appeared in stark contrast to the canonical cellular
271 localization of the M_2 receptor, as shown in **Fig. 4b** where the M_2 muscarinic receptor was C-terminally labeled
272 with the red fluorescent protein mRuby2. Interestingly, very little expression of M_2tail(368-466)-EGFP was
273 observed on the plasma membrane, as we confirmed by fluorescence correlation spectroscopy[14]
274 (**Supplementary Fig. 7b-d**). By contrast, when the M_2tail(368-466)-EGFP was co-expressed with M_2stop228,
275 a modest localization could eventually be detected also on the cell membrane thanks to a reduction in diffusion
276 coefficient of M_2tail(368-466)-EGFP, suggesting a chaperon activity of the M_2 N-terminal domain (M_2trunk)
277 (**Supplementary Fig. 7e-g**) and hence explaining the [^{3}H]NMS binding observed in cells transfected with
278 either M_2stop228 or cotransfected with M_2trunk(1-228) and M_2tail(368-466) (**Table 1**). Likewise, constructs
279 such as M_2tail(368-466)-mRuby2 (a red monomeric fluorescent protein) and M_2tail(368-466)-tdTomato (a

280 tandem-dimer red fluorescent protein) also displayed clear mitochondrial localization (**Supplementary Fig.**
281 **7h-i**), ruling out bias due to the fluorophore used.
282
283 **Localization of the M_2 C-terminal fragment generated by cap-independent expression under the control**
284 **of the i3loop IRES**.
285 We then sought to express the C-terminal fragment of the M_2 receptor under the control of the i3loop IRES
286 rather than a viral promoter, to further exclude the possibility that the observed localization of the M_2 carboxyl
287 terminal fragment were due to overexpression of the construct. HEK293 cells were transfected with the
288 construct M_2-mRuby2-STOP-M_2-i3-tail-EGFP which contains the full wild type M_2 receptor, mRuby2-labeled
289 at the C-terminal, fused to the C-terminal part of the M_2 receptor starting at nucleotide 685 of the i3 loop,
290 following the stop codon of mRuby2, and ending with a C-terminal EGFP sequence. Through this experimental
291 strategy, the expression of M_2tail(368-466)-EGFP is regulated by the IRES, and the mechanism of C-terminal
292 fragment production is therefore close to physiological. The expression of EGFP confirmed that the *in vivo*
293 production of the M_2tail(368-466) is regulated by the IRES within the i3 loop. In addition, the processed
294 receptor fragment was eventually observed to be predominantly confined to the cytosol and the mitochondrial
295 network (**Fig. 4c**).
296 Notably, when the M_2-EGFP fusion protein was expressed and the cells were co-stained with Mitotracker, a
297 faint EGFP signal was also observed in the mitochondrial regions (**Supplementary Fig. 8a**), although the
298 expression of the full-length receptor masks this effect and makes quantification difficult. On the other hand,
299 **Fig. 4d** shows that, when the M_2fr.sh-EGFP mutant was expressed in HEK293 cells, the IRES generated C-
300 terminal fragment of the M_2 receptor still localized to the mitochondria. As mentioned above, in this construct
301 the masking effect of the EGFP fused to the full-length receptor is removed (see also **Supplementary Fig. 1**).
302 Similar mitochondrial localization was also observed when we transfected HEK293 cells with M_2fr.sh-
303 mRuby2 (**Supplementary Fig. 8b**), ruling out possible effects due to the specific fluorophore used as a tag.
304 We obtained comparable findings also in COS-7 cells (**Supplementary Fig. 8c**).
305 Mitochondrial import of the C-terminal fragment of the M_2 receptor was further verified by immunoblotting
306 of protein extracts from purified mitochondria of HEK293 cells transfected with myc-tagged M_2 receptor,
307 M_2tail(368-466) and M_2M368A. **Fig. 4e** shows that in purified mitochondria (unlike in the cytosolic and

308 microsomal supernatants originating from the purification process, **Supplementary Fig. 8d**), only the protein
309 bands associated to the M_2 C-terminal fragment were visible.
310 Notably, no mitochondrial import was visible for the M_2M368A, confirming that the third in frame methionine
311 (M368) in the i3 loop of the M_2 receptor is necessary for the C-terminal fragment production and its localization
312 in the mitochondria.
313 A consistent result was observed when mitochondria were purified from the heart and spleen of the
314 Chrm2/tdtomato mice **Fig. 4f** (the cytosolic fraction is shown in **Supplementary Fig. 8e**). A band at ~75 kDa,
315 matching the molecular weight of the M_2 C-terminal domain, was clearly visible. We conclusively confirmed
316 that this is the fingerprint associated to the M_2 C-terminal fragment, by purifying mitochondria from HEK293
317 cells expressing the construct M_2tail(368-466)-tdtomato. **Fig. 4g** (cytosolic fraction is shown in
318 **Supplementary Fig. 8e)** shows a ~75 kDa protein band matching closely the bands observed in mitochondria
319 from mice tissues, in addition to lower molecular weight bands most likely arising from degradation of the
320 tdtomato tag.
321 Mitochondrial localization of the M_2tail originating from the wild type M_2 receptor was finally confirmed by
322 relative abundance estimates of EGFP and M_2 receptor from parallel reaction monitoring (PRM)-based mass
323 spectrometry measurements **Supplementary Fig. 9**. Samples were prepared by generating mitochondrial and
324 cytosolic fractions (**Methods**) from HEK293 cells, expressing M_2-EGFP and a set of control constructs,
325 including M_2tail(368-466)-EGFP, pmito-EGFP (an EGFP fused to the mitochondrial leading sequence of the
326 cytochrome c oxidase subunit 8A (COX8A)), lifeact-EGFP (a cytosolic protein) and Epidermal Growth Factor
327 receptor fused to EGFP (EGF-EGFP). A 15-aminoacid long peptide originating from EGFP was screened. The
328 bands intensities of the cytosolic fraction, were normalized to consider both the overall loading variability as
329 well as the relative transfection efficiencies among the samples. Notably, we observed a mitochondrial
330 enrichment of the EGFP derived peptide as well the receptor-specific peptide originating from the M_2 receptor,
331 in agreement with the positive mitochondrial localization control.
332

333 **Mechanism of import of the M_2 carboxyl terminal fragment into the mitochondria and localization**
334 **within the organelle**

335 To gain further insight into the dynamics of the M_2 C-terminal fragment import within the mitochondria, we
336 first monitored the kinetics of colocalization between mitochondria and EGFP in cells transfected with
337 M_2tail(368-466)-EGFP. In cells observed for several hours, starting at 5h after transfection (**Fig. 4h)**, the
338 construct was found initially expressed in the perinuclear region, likely the endoplasmic reticulum, indicating
339 that at least the initial step of subcellular trafficking of the M_2tail(368-466)-EGFP is the same as for the full
340 length receptor[15]. At this time (5h post-transfection), almost no colocalization with the Mitotracker-stained
341 mitochondria was visible. However, at 6h post-transfection, the colocalization level increased significantly,
342 and the M_2 C-terminal fragment was either found in the cytosol or in the mitochondria. At 9h post-transfection
343 the colocalization at the mitochondria was well visible. We quantified the colocalization level over time using
344 the Manders' coefficients (See **Methods**). The resulting chart, indicates that almost half of the mitochondrial
345 import occurred within 6h post-transfection.
346 This value is qualitatively in agreement with what we observed using an in-vitro assay to determine the import
347 of the M_2 carboxyl terminal into isolated mitochondria (see Methods). To this end, we used mitochondria form
348 *S. cerevisiae*, which is a robust and well-studied system for protein import assays. **Supplementary Fig. 10a**
349 shows the autoradiography experiment of isolated, intact, mitochondria incubated with 35S-labelled full length
350 muscarinic M_2 receptor or M_2tail(368-466), made using a reticulocyte in vitro translation system. The data
351 show that the full-length receptor was not imported into mitochondria. On the other hand, the M_2tail(368-466)
352 displays a clear mitochondrial import already after 5 minutes and increasing over time, up to 30 minutes.
353 Interestingly, this import (**Supplementary Fig. 10b)** appears to be independent upon the transporters of the
354 outer membrane Tom5, Tom6, Tom7 and Tom70, whereas the import of an inner membrane protein, the
355 ADP/ATP carrier (AAC), used here as a control, depends on Tom70. Upon extraction with carbonate most of
356 M_2tail(368-466) was found in the pellet, and therefore presumably integrated in a membrane. Furthermore Blue
357 native analysis suggests that the mitochondrially imported M_2tail(368-466) is not a monomer but rather it is
358 part of a larger complex of approximately 180 kDa **Supplementary Fig. 10c.**
359 All together these data indicate that the import of the M_2tail(368-466) leads to its localization in one of the
360 mitochondrial membranes, to form a complex with other native mitochondrial proteins.
361

362 To further discriminate if the construct is on the outer or inner mitochondrial membrane, we set up a
363 fluorescence assay based upon GFP fluorescence complementation[16]. HEK293 cells were first transfected with
364 two constructs: M_2tail(368-466)-GFP11, in which a short 16 amino acids peptide of GFP was fused at the C-
365 terminus of M_2tail(368-466), and mito-GFP1-10, in which the COX8A was N-terminally fused to the other
366 GFP fragment containing the remaining 10 beta strands (See **Methods**). **Supplementary Figure 10d** shows
367 the successful recombination of the two within the mitochondrial matrix. We then applied this approach to the
368 full length M_2 receptor, by generating the M_2-GFP11 construct and by transfecting it in HEK293 cells. **Fig. 4i**
369 shows a green signal from the recombined GFP visible in the mitochondria. All together these data suggest
370 that the M_2 C-terminal fragment is localized in the inner mitochondrial membrane, with its own C-terminal
371 domain facing the matrix.
372 This interpretation appears to be confirmed in cells expressing the M_2stop228-myc receptor and examined by
373 electron microscopy (**Supplementary Fig. 10e**) after immune-gold labelling. As shown in **Supplementary**
374 **Fig. 10f-g**, gold particles were observed only in mitochondria, and at this stage they appeared localized either
375 to the mitochondrial matrix or to the lumen of the cristae (**Supplementary Fig. 10h-k)**.
376

377 **Functional role of the C-terminal fragment in the mitochondria**

378 The next step of our investigation concerned the obvious question about the functional effects, if any, that the
379 observed localization of the M_2 C-terminal fragment might have on the mitochondrial activity, and -more
380 generally- on the energy metabolism of the cell. To investigate this aspect, we measured the extent of oxygen
381 consumption in COS-7 cells expressing M_2-EGFP, M_2tail(368-466)-EGFP or the sole EGFP as a control.
382 Initially, we normalized the expression of the three proteins to the amount of EGFP expressed in the cells, then
383 the metabolic functions were assayed on a Seahorse instrument using cells transfected with normalized
384 amounts of plasmids **(Fig. 5a)**.
385 Our data did not show a significant difference in total oxygen consumption capacity between cells transfected
386 with cytosolic EGFP and the untransfected control. However, a significant decrease of oxygen consumption
387 was found in cells transfected with M_2-EGFP and even more so with M_2tail(368-466)-EGFP (**Fig. 5a**). Notably,
388 the basal oxygen consumption rate (OCR), in starvation-stress conditions, was profoundly decreased in
389 M_2tail(368-466) cells and to a smaller extent in M_2 cells compared to EGFP and empty control cells (see also

390 the time-course in **Supplementary Fig. 11a)**. These results are in line with what was observed using a Clarke-
391 type oxygen electrode (**Supplementary results and Supplementary Fig. 11b and 11c**).
392 A cell apoptosis assay, based on the detection of activated caspase-3[17], did not show substantial differences
393 among the tested mutants (**Supplementary Fig. 11d**). The overexposed western blot showed a tiny amount of
394 activated caspase-3 in most of the transfected COS-7 cells, indicating that the expression of M_2tail(368-466)
395 in mitochondria, in agreement with the qualitative post-starvation data shown in **Supplementary Fig. 11e**,
396 does not induce fragmentation of the mitochondrial network and cell apoptosis.
397 To test whether the C-terminal-M_2 fragment effects on mitochondrial oxygen consumption could alter the
398 production of Reactive Oxygen Species (ROS), the measurements were combined in a single cell assay.
399 Remarkably, ROS production (assayed using a fluorescence readout kit, where the fluorochrome becomes
400 activated in contact with oxidized species) was clearly reduced within and in proximity of mitochondria of
401 cells expressing a high level of the M_2tail(368-466) (**Fig. 5b**). By regrouping individual mitochondria in classes
402 according to the level of the ROS marker expression, an actual inverse correlation between the amount of
403 receptor fragment (Green Fluorescence) and the production of ROS (Red Fluorescence) was revealed.
404 Cell growth was also found to be affected depending on which of the constructs was transfected. Notably,
405 transfection of HEK293 cells with the wild type M_2 receptor reduced significantly cell growth compared to the
406 control, whereas cells transfected with the mutant M_2M368A, that do not express the M_2 C-terminal fragment
407 (**Fig. 5c**), displayed a significantly higher growth. All cells were incubated with saturating concentration of the
408 M_2 antagonist atropine throughout, in order to exclude effects on cell growth and proliferation due to the
409 canonical receptor signaling.
410

411 **Cell stress upregulates M_2 C-terminal expression and mitochondrial localization**

412 Having established that the C-terminal fragment localizes in the mitochondria and affects the cell oxygen
413 consumption rate, we looked at the effect of stress on the level of expression of the C-terminal fragment.
414 Stressed cells attenuate their translational activity via phosphorylation of the initiation factor eIF2α. However,
415 certain mRNAs may be insensitive to eIF2α phosphorylation level if their translation is regulated by IRES.
416 Under these conditions their expression is bound to increase rather than to attenuate [18,19].

417 Therefore, we transfected COS-7 cells with the Sirius-M_2i3(417n)-EGFP reporter construct and stressed by
418 starvation for three hours by replacing the culture medium with HBSS or PBS. During this time interval, the
419 green fluorescence was seen to gradually increase up to 1.4 times the basal level observed in HBSS-starved
420 cells and 3.5 times for PBS-starved cells (**Fig. 5d**), confirming that the C-terminal fragment expression is
421 upregulated in response to stress conditions such as cell starvation. The same experiment was reproduced in
422 single cells, displaying an increase of the average EGFP/Sirius ratio upon HBSS starvation in HEK293 cells
423 (**Fig. 5e**).
424 We further used the GFP fluorescence complementation assay to emphasize the importance of stress in the
425 pattern of expression of the M_2 gene. HEK293 cells were co-transfected with M_2-GFP11 and Mito-GFP1-10.
426 HEK293 cells grown in culture medium predominantly expressed the full M_2 receptor protein (**Fig. 5f**). The
427 green fluorescence detected in the plasma membrane is explained with the chaperoning effect of M_2-GFP11
428 on Mito-GFP1-10 before its sorting to the mitochondria. In sharp contrast, when HEK293 cells were first
429 transfected with Mito-GFP1-10 and, 24h later, transfected with M_2-GFP11 followed by a 6 h starvation in
430 HBSS, the pattern of expression changed drastically: IRES mediated translation of the M_2tail(368-466)
431 fragment led to a predominantly mitochondrial green fluorescence signal of the complemented GFP (**Fig. 5f**).
432 These results are in line with our observation that the IRES mediated C-terminal fragment localization to the
433 mitochondria in cells expressing the construct *M_2-mRuby2-STOP-M_2-i3-tail-EGFP* was enhanced upon cell
434 starvation, and drastically reduced upon mutation of the M368 (**Supplementary Figure 12** and
435 **Supplementary Methods**).
436 This observation was also supported by the lack of complementation of M_2tail-GFP11 with GFP1-10 when
437 this last fragment was N-terminally fused to the targeting sequence of SMAC, a protein expressed in the
438 mitochondrial intermembrane space [20] (**Supplementary Fig. 13c**).
439

440 **Mutation of the M368A via CRISPR/Cas9 affects cell growth and oxygen consumption rates in hiPSCs**
441 We finally asked the question of what would be the effect of abolishing the translocation of the M_2 C-terminal
442 fragment to the mitochondria, in a physiological and entirely label-free setting. To reach this goal we
443 genetically engineered (see Methods) human induced pluripotent stem cell (hiPSC), to incorporate in both
444 alleles of the M_2 gene the M368A mutation, that, based on our data, should be sufficient to significantly impair

445 the M_2 C-terminal production and mitochondrial translocation. Wild typ (wt)e and M368A hiPSCs were
446 cultured in pluripotency maintaining medium, and subsequently undirectedly differentiated upon exposure for
447 seven days to DMEM-F12 medium, as described in the Methods. **Fig. 6a** shows confocal micrographs for wild
448 type and M368A hiPSCs cultured in E8 medium respectively, with the M368A hiPSCs displaying a mildly
449 more spread-out phenotype. We shall note here that the M_2 receptor has been found to be expressed in PSCs
450 lines, and it has been shown to play a role in stem cell differentiation [21,22]. In this context, however, we were
451 not interested in the canonical signaling of the receptor, and all experiments were performed with a saturating
452 concentration of atropine, to block any activity of the receptor. We then evaluated cell proliferation, observing
453 a significant increase in the proliferation of the M368A clone 72h after seeding **Fig. 6b**. The observation of an
454 increased proliferation of the cells harboring the mutation that impairs the production and localization of the
455 C-terminal fragment in the mitochondria, suggests that the same effect is at play here, as observed in the
456 overexpression system (**Fig. 5a,b,c**). These results are supported by extracellular oxygen consumption assays
457 performed, for both hiPSCs and differentiated hiPSCs (**Fig. 6c**). Our data suggest that the M368A cells indeed
458 display an accelerated oxygen consumption rate, and that this effect increases as the cell progressively
459 differentiates.
460 For comparison, the assay was also carried on HEK293 overexpressing the wild type M_2 receptor and the
461 mutant M_2M368A (**Supplementary Fig. 11f**). We could observe with this assay a reduced oxygen
462 consumption of the wild type M_2 receptor compared to untransfected cells, in line with what was observed in
463 **Fig. 5a**, and an increased oxygen consumption of the M_2M368A expressing cells, in line with what observed
464 for the hiPSCs.
465

466 **Discussion**

467 Over the last 10 years, growing evidence has accumulated indicating that GPCRs can be functional and signal
468 also at cellular locations other than the plasma membrane. These locations can be associated to their canonical
469 trafficking pathways (such as sorting vesicles and endosomes)[23], but also to non-canonical locations, such as
470 the nucleus, the nuclear membrane, the Golgi apparatus and the mitochondria (reviewed in Jong et al. BPJ
471 2018 [24]). Some of these locations are surprising, since many ligands are non-membrane permeable, and it is
472 still debated how they can reach their target receptors at such intracellular locations.

473

474 Interestingly, the specific localization of these receptors appears to go hand in hand with a specific function.
475 In these cases, activation/inhibition of mitochondrially localized GPCRs have been shown to specifically affect
476 the organelle function, ranging from oxygen consumption rates to Ca^{2+} handling and even to apoptosis. Notably
477 Benárd et al [25] showed that the CB_1R on the outer mitochondrial membranes affects neuronal energy
478 metabolism; Suofu et al. [10] demonstrated that activation of the MT_1R by a mitochondrial melatonin pool can
479 affect cytochrome C release. This is particularly interesting, since cytosolic cAMP does not appear to be able
480 to activate mitochondrial PKA, and hence a mitochondrially localized GPCR signalosome appears to be
481 required to enable such downstream signaling cascade [26].

482

483 However, other non-canonical mechanisms are also possible for the regulation of mitochondrial function. It is
484 well known that GPCRs are subject to interindividual variability, arising, for example, from mRNA alternative
485 splicing (i.e. the process which allows the recombination of exons) which leads to different isoforms which
486 may present distinct signaling and localization properties [27]. Receptor variants with different functional and
487 localization properties may also occur due to other processes. For example, our comprehension of eukaryotic
488 translational regulation is facing a rapid expansion, as exemplified by the observation that small open reading
489 frames (smORFs), also within lncRNAs, are an important class of genes, oftentimes with mitochondrial
490 localization[28].

491

492 In this study, for the first time, we provide evidence that an IRES sequence drives expression of a membrane
493 receptor fragment and acts as a regulator of its expression levels and function. IRES sequences are distinct
494 regions of the mRNAs that are capable of recruiting ribosomes in the proximity of an internal initiation codon
495 and translate transcripts in a cap-independent manner [5,6,29-31]. Here, we show that an IRES sequence is located
496 within the third intracellular loop of the M_2 muscarinic receptor, where it plays a crucial role in regulating the
497 expression of its carboxy-terminal domain, which we identified as M_2tail(368-466).

498

499 We assessed the IRES-driven expression of the C-terminal fragment through a broad set of constructs, meant
500 to exclude alternative synthesis mechanisms such as stop-codon read-through, and a diversified palette of

501 techniques. Radioligand binding data (**Table 1**) pointed to the necessity of the C-terminal fragment synthesis,
502 in order to explain the observed downstream signaling in mutants carrying a stop codon in the initial portion
503 of the i3loop of the M_2 receptor, upstream of M368. Fluorescence microscopy allowed us visualizing the
504 production of the EGFP-tagged C-terminal fragment in these receptor mutants (**Fig. 1d**). We further detected
505 its production by Western blotting on protein extracts from cells; here the C-terminal fragment gives rise to
506 two bands: the lower of the two (~15 kDa) appears to be proportional to the ~75 kDa band, suggesting that this
507 may result from subsequent processing or degradation. On the other hand the ~20 kDa band intensity appears
508 independent of the M_2 full-length band (~75 kDa), as would be expected for a cap-independent translation
509 mechanism, and this band disappears in the M368A mutant.
510 We further performed Western blotting from heart and brain tissues from knock-in mice carrying a C-
511 terminally tagged M_2 receptor (tdtomato) and under the control of the endogenous promoter/enhancer
512 sequences (**Fig. 2a-c**).
513
514 Mutagenesis of key residues within the i3 loop of the M_2 receptor allowed us to pinpoint the 3rd in-frame
515 methionine as the most likely candidate for the beginning of the cap-independent translation (**Fig. 3**). This
516 observation appears to be supported by the observation of a peak in ribosome coverage around the M368 seen
517 in ribosome profiling databases (as reviewed in Ingolia et al.[32]), and particularly prominent in those from left
518 ventricle cardiomyocytes, where M_2 receptor expression is known to be abundant[28].
519
520 To our surprise, in contrast to the plasma membrane localization of the wild type, full length M_2 receptor, the
521 C-terminal fragment was localized mostly in mitochondria. This localization occurred markedly when
522 overexpressing the C-terminal fragment M_2tail(368-466), but could be also clearly detected when the C-
523 terminal fragment was expressed under the control of the IRES sequence of the full length receptor (**Fig. 4**
524 **c,d**).
525
526 We devised several strategies to detect the localization of the IRES-driven fragment in the mitochondria by
527 avoiding the cell-wide background signal from the full-length receptor. **Fig. 4c,d** show two prominent
528 examples, namely relying on spectrally unmixing the two components, or by sending out of frame the EGFP

529 at the C-terminus of the full-length receptor. By studying mitochondria purified from HEK293 cells we could
530 confirm that the mutation of the M368, which we identified as the starting point of the IRES-mediated
531 translation, is sufficient to suppress any mitochondrial targeting of the M_2 C-terminal fragment, and most
532 likely, its synthesis altogether (**Fig. 4e**).
533
534 We then addressed the mechanism of mitochondrial import of the C-terminal fragment and its localization
535 within the organelle. Our data, originating both from live cell import kinetics (**Fig.4h**) as well as from in-vitro
536 import into isolated mitochondria (**Supplementary Fig. 10**), support the notion that the fragment becomes
537 rapidly imported into mitochondria following translation in the cytosol. Once inside the mitochondria, it
538 undergoes processing leading to the appearance of a lower molecular weight band, observed both in Western
539 blots from whole cell and mice tissue protein extracts, as well as from purified mitochondria. The fragment is
540 found predominantly in a carbonate-insoluble fraction, i.e. a membrane, and it appears to form a high molecular
541 weight complex of ~180 kDa with other mitochondrial proteins (**Supplementary Fig. 10c**).
542 Fluorescence complementation assays (**Fig. 4i**) and electron microscopy (**Supplementary Fig. 10d**) suggest
543 that the M_2 C-terminal fragment predominantly resides in the inner mitochondrial membrane, with its own C-
544 terminal domain exposed towards the matrix. Future work should clarify the precise import pathway.
545
546 Most importantly, our data show that mitochondrial oxygen consumption was reduced by the M_2tail(368-466)
547 (**Fig. 5a,b**), and also cell proliferation was affected (**Fig. 5c**). Under integrated stress response, namely
548 aminoacid starvation, IRES-mediated production of the C-terminal fragment was increased (**Fig. 5d-f**). On
549 these bases, the M_2tail might be needed in mitochondria as a means to reduce mitochondrial basal oxygen
550 consumption and ATP-linked respiration. An important consequence of reduced respiration is the lower level
551 of ROS produced in mitochondria, as we observed in agreement with this hypothesis.
552 This observation was confirmed in physiological, label-free conditions, by genetically editing human induced
553 pluripotent stem cells in order to suppress the synthesis of the M_2 C-terminal fragment mutating the starting
554 methionine M368. Increase of cell proliferation of this clone compared to its wild type counterpart, together
555 with an increase of oxygen consumption rates (**Fig. 6**), corroborates our hypothesis that the M_2 C-terminal
556 fragment reduces oxygen consumption upon reaching the mitochondria. The effect was further amplified when

557 the cells were undirectedly differentiated, and it was consistent with the shift of the cell phenotype towards
558 oxidative phosphorylation[33].
559
560 The mechanism by which the M_2tail(368-466) may reduce oxygen consumption in mitochondria and its
561 meaning needs to be further explored. Nonetheless, since ROS production is implicated in the pathogenesis of
562 several diseases[34], we would propose the hypothesis that increased localization of the M_2 C-terminal fragment
563 in mitochondria, as it occurs under integrated stress response, might have protective effects (**Fig. 7**).
564
565 In broader terms, protection of mitochondria by unconventional import mechanisms to allow localization
566 within the organelle of specific proteins has been previously observed for cells that undergo stress conditions
567 [35]. The mechanism of IRES-dependent modulation of translation and consequent mitochondrial targeting of
568 the translation product of a GPCR may provide another means, completely unrelated to the canonical signaling
569 function of this class of membrane receptors, of a generic cellular response to overcome different types of
570 stress by modulating the mitochondrial proteome and adjusting the mitochondrial bioenergetic state.

571 **Tables, Figures and Supplementary Tables and Figures**

572 **Table 1. Radioligand binding and activation properties of M_2 receptor mutants.** Binding properties and inhibition of
573 forskolin stimulated adenylyl cyclase by M_2, M_2stop228 and the co-transfected M_2trunk(1-283)/M_2tail(M-281-466) and
574 M_2trunk(1-228)/M_2tail(368-466). Untransfected COS-7 cells did not show any [^{3}H]NMS specific binding. N.B. = no
575 specific [^{3}H]NMS binding.

Binding data				Adenylyl cyclase inhibition assay	
Receptor	Bmax (fmol/mg)	[^{3}H]NMS KD (pM)	Carbachol IC50 (µM)	Carbachol EC50 (µM)	Maximum inhibition of forskolin stimulated cAMP accumulation (%)
M_2	980 ± 60	62 ± 7	2.1 ± 0.6	0.04 ± 0.01	53 ± 5
M_2trunk(1-283)	N.B.				
M_2trunk(1-228)	N.B.				
M_2stop228	45 ± 2	70 ± 10	1.8 ± 0.4	0.13 ± 0.02	27 ± 3
M_2trunk(1-283) +M_2tail(M-281-466)	480 ± 20	79 ± 10	0.7 ± 0.2	0.15 ± 0.03	37 ± 4
M_2trunk(1-228) +M_2tail(368-466)	70 ± 10	72 ± 8	0.6 ± 0.2	0.17 ± 0.03	29 ± 4

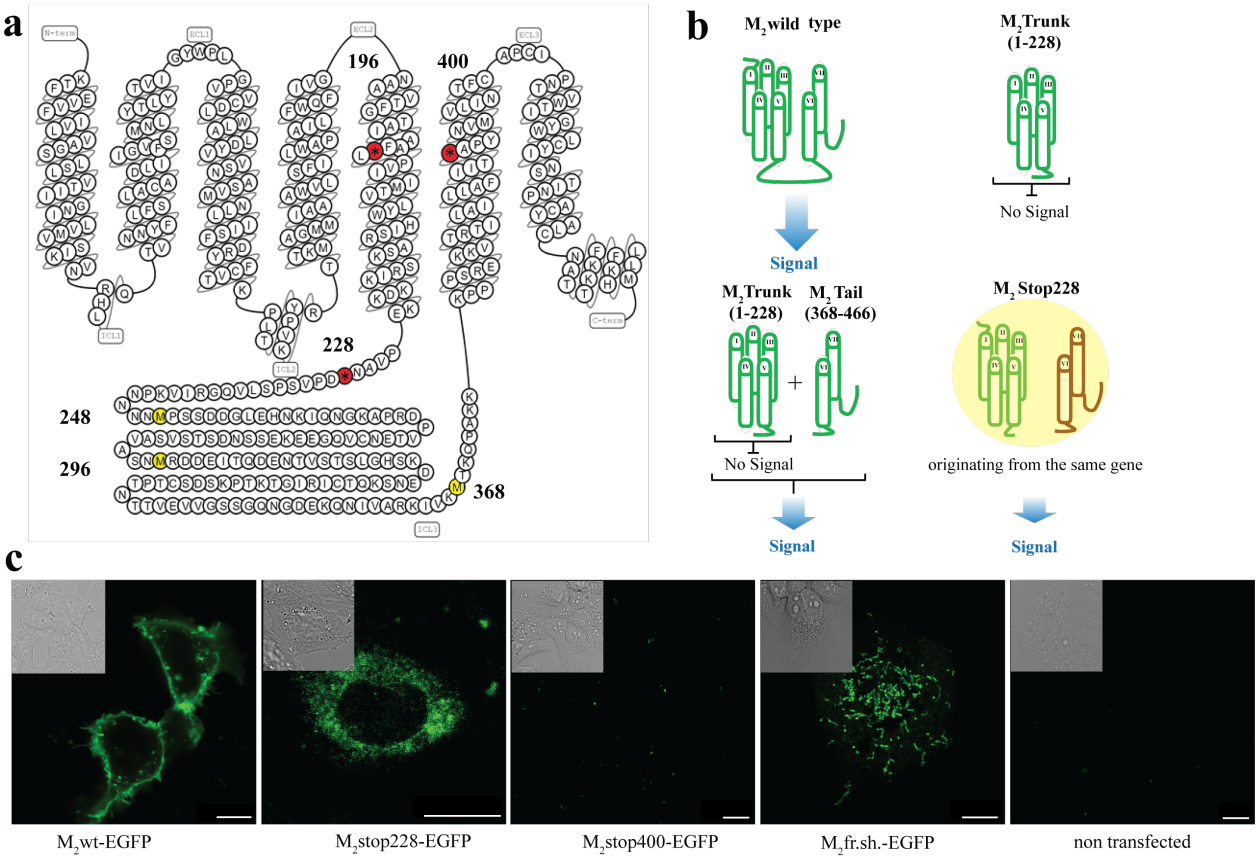

Fig. 1. Mutations of the M_2 receptor confer unexpected functional and localization properties. **a**, Snake-like plot of the human muscarinic M_2 receptor: in red are indicated the aminoacids substituted with stop codons in the mutants: M_2stop196, M_2stop228 and M_2stop400 (**Supplementary Fig. 1**). The three in-frame methionines of the i3 loop, 248, 296 and 368, are highlighted in yellow; the translation of the C-terminal fragment starts from methionine 368. **b**, Schematic representation of the gene products that reach the plasma membrane of the wild type M_2, M_2trunk, M_2trunk and M_2tail and M_2stop228 (**Supplementary Fig. 1**). The M_2trunk and M_2tail genes generate the respective protein fragments that, only when co-transfected together, are able to form functional receptor complexes capable to bind ligands. The M_2stop228 gene mutant generates both M_2trunk (in green), when translation starts from the cap site, and M_2tail (in brown) when translation is cap-independent driven. This makes it likely that the truncated fragment of the M_2stop228 receptor may act as a chaperon driving part of the C-terminal-M_2 fragment to the plasma membrane, as supported by the binding and functional data shown by the co-transfection of M_2trunk(1-228) with M_2tail(368-466) (**Table 1**). **c**, Fluorescence micrographs of HEK293 cells respectively expressing M_2-EGFP, M_2stop228-EGFP, M_2fr.sh.-EGFP and M_2stop400-EGFP, together with an untransfected control. Imaging settings are the same for the five images, whereas contrast was adjusted to improve visualization. In the untransfected cells and stop400 panels, the contrast was set to 0. Insets display DIC image of the same field of view (scale bars 10 µm).

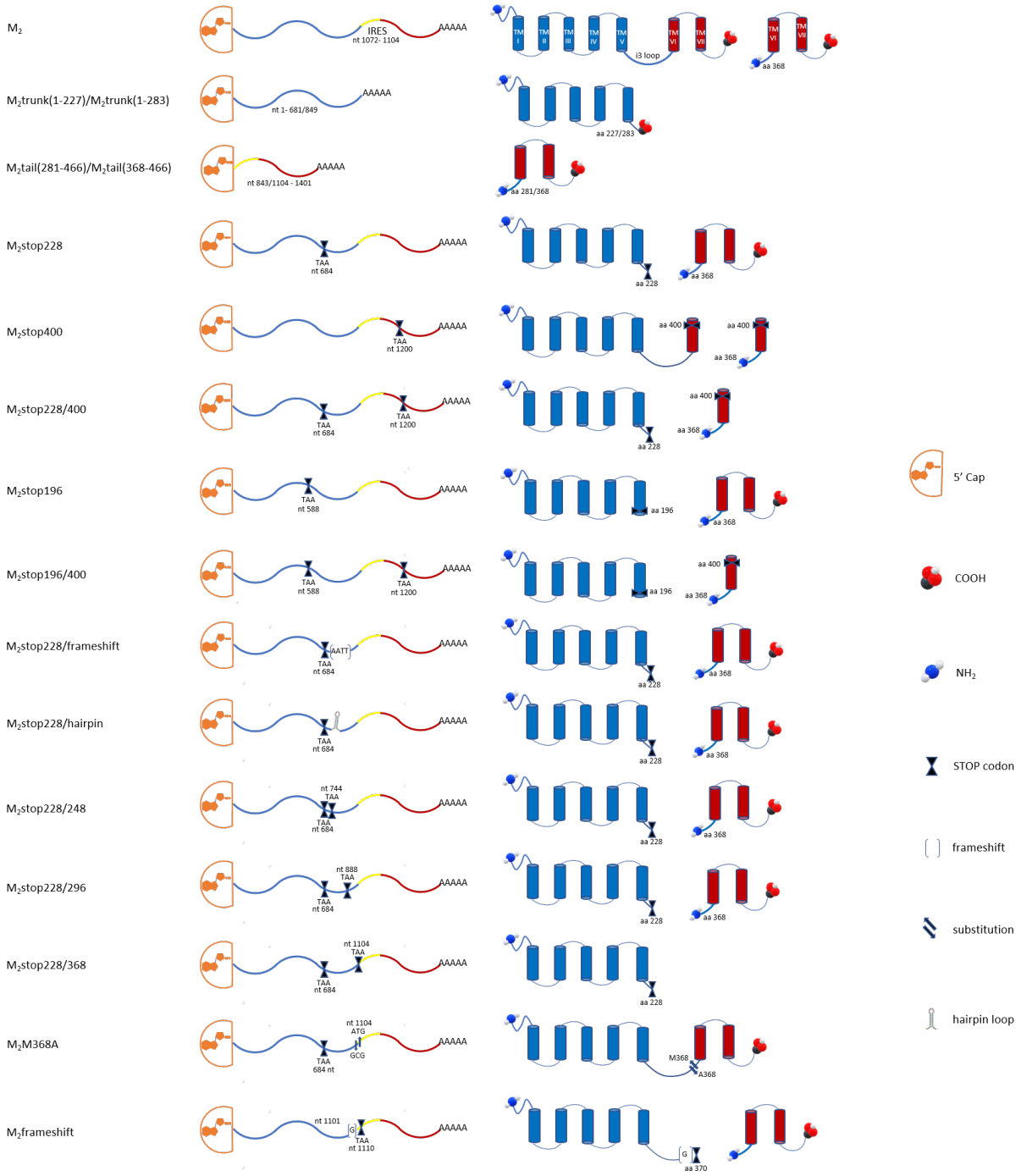
M2
IRES
nt 1072- 1104
AAAAA
TM I
TM II
TM III
TM IV
TM V
TM VI
TM VII
i3 loop
aa 368
M2trunk(1-227)/M2trunk(1-283)
nt 1- 681/849
aa 227/283
M2tail(281-466)/M2tail(368-466)
nt 843/1104 - 1401
aa 281/368
M2stop228
TAA
nt 684
aa 228
M2stop400
nt 1200
aa 400
M2stop228/400
M2stop196
nt 588
aa 196
M2stop196/400
M2stop228/frameshift
AATT
M2stop228/hairpin
M2stop228/248
nt 744
M2stop228/296
nt 888
M2stop228/368
nt 1104
M2M368A
ATG
GCG
684 nt
M2frameshift
nt 1101
G
nt 1110
aa 370
5' Cap
COOH
NH2
STOP codon
frameshift
substitution
hairpin loop
M2-mRuby2-Stop-M2i3-tail-EGFP
mRuby2
nt 687
GAC
EGFP
Stop
M2(M368A)-mRuby2-Stop-M2i3-tail-EGFP
M368
A368

593

Supp. Fig. 1. Schematic representation of wild type muscarinic M_2 (human) receptors and derived mutants. Each construct was obtained as described under **Methods**. The left column indicates the mRNA product from each construct, the right column the expected protein product. For the last two constructs, above mRNA product, and below the expected protein product.

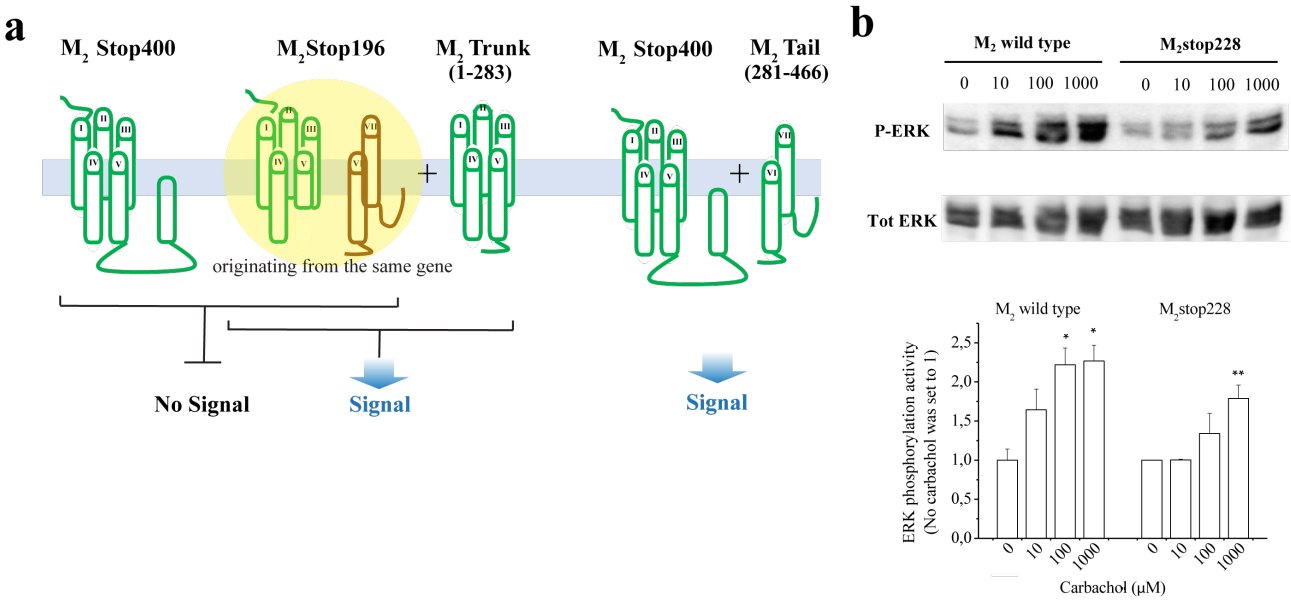

Supp. Fig. 2. M_2 receptor mutants with single and double stop codons. a, Schematic representation of the gene products M_2stop196 and M_2stop400, that are not functional by themselves but that are rescued by co-transfection with M_2Trunk(1-283) and M_2Tail(M-281-466), respectively. **b**, Dose response curve of carbachol induced ERK phosphorylation in HeLa cells transiently transfected with M_2 and M_2stop228 muscarinic receptors. Cells were stimulated for 5 minutes with the indicated concentration of carbachol. Phosphorylated ERK (P-ERK) was normalized vs total ERK (Tot ERK). Significance (*$p < 0.05$, **$p < 0.01$) was calculated against carbachol 0 μM.

Supplementary Table 1. Ligand binding and functional properties of M_2 receptor mutants with single and double stop codons. Number of [^{3}H]NMS binding sites for the indicated mutants. Untransfected COS-7 cells did not show any [^{3}H]NMS specific binding. N.B. = no specific [^{3}H]NMS binding.

Receptor	Bmax (fmol/mg)	Receptor	Bmax (fmol/mg)
M_2stop228	45.3 ± 2.4	M_2stop228/stop368	N.B.
M_2stop196	N.B.	M_2stop228/stop368 + M_2tail(281-466)	370± 20
M_2stop400	N.B.	M_2stop228/stop400	N.B.
M_2stop196+ M_2trunk(1-283)	47 ± 3	M_2stop228/stop400+ M_2tail(281-466)	380 ± 20

M_2stop400+ M_2tail(281-466)	400 ± 30	M_2stop196/stop400+ M_2trunk(1-283)	N.B.
M_2stop196/stop400	N.B.	M_2stop196/stop400+ M_2tail(281-466)	N.B.
M_2stop228/stop248	49 ± 5	M_2stop228/fr.sh.	47 ± 3
M_2stop228/stop296	38 ± 3	M_2stop228/Hairpin	37 ± 2

608

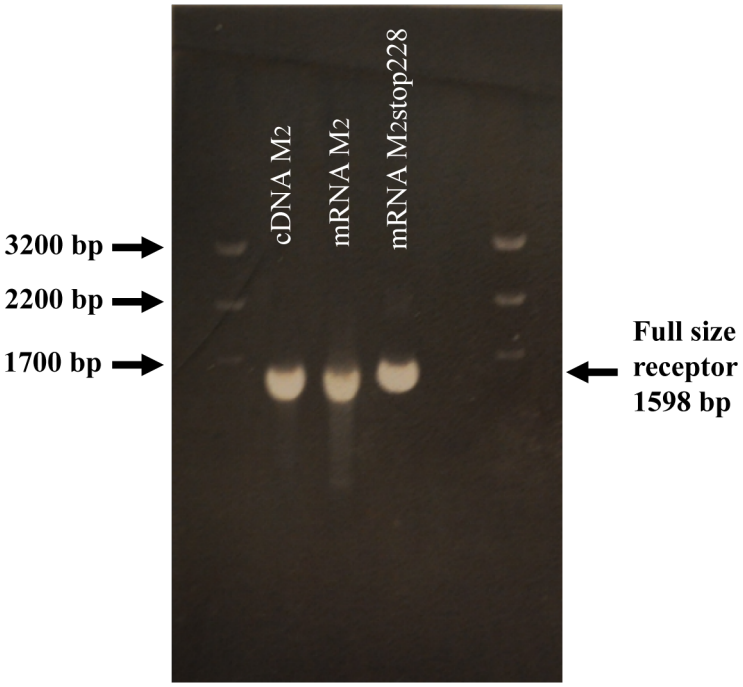

609

610 **Supp. Fig. 3. Lack of alternative splicing in M_2 wild type and M_2stop228 receptors**. mRNAs were extracted by COS-
611 7 cells transfected with M_2 wild type and M_2stop228, subjected to reverse transcriptase and the resulting cDNA amplified
612 by PCR with two oligos directed to the 5' and 3' end of the receptors. The gel shows, in both M_2 wild type and M_2stpo228,
613 a single band of 1401 bp corresponding to the full-size receptor, running at the same level of the band amplified directly
614 form the M_2 pcD plasmid.

615

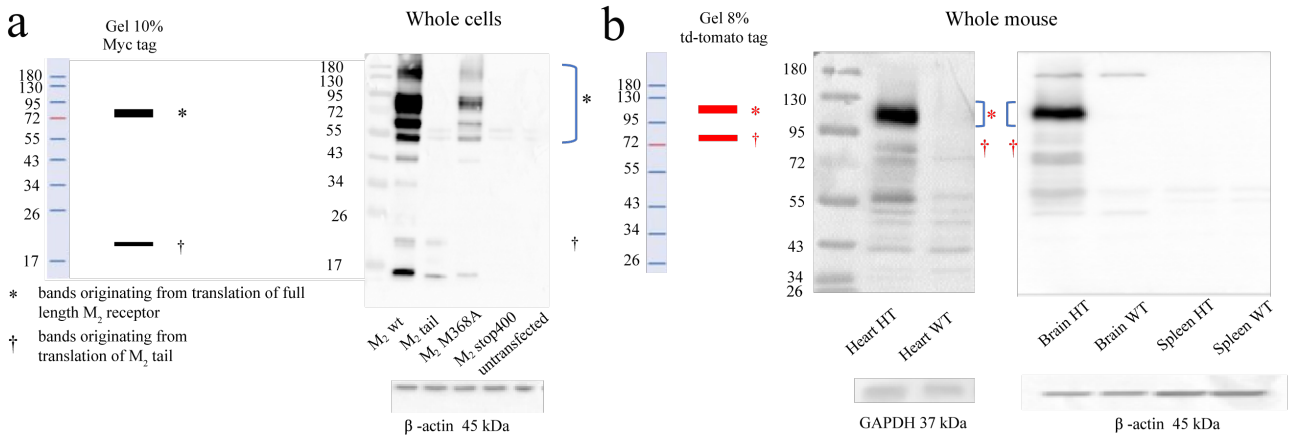

Fig. 2. Western blot of tagged M_2 receptor mutants in HEK293 cells and in tdtomato knock-in mice. a, left Graphical guide of the fragments observed on the gel when using myc-tag. **right**, M_2-myc, M_2tail(368-466)-myc, M_2M368A-myc and M_2stop400-myc were transiently transfected in HEK293 cells and immunodetected via antimyc primary antibody, together with an untransfected control. Loading control normalization was performed vs β-actin **b**, **left** Graphical guide of the fragments observed on the gels when using the tdtomato tag. **right**, Western blot from tissue preparations originating from the indicated organs of M_2-tdtomato knock-in mice (HT) and wild-type animals (WT). Immunodetection was performed using an anti-tdtomato primary antibody. Loading control normalization was performed using GAPDH in the heart, and β-actin in the brain and spleen.

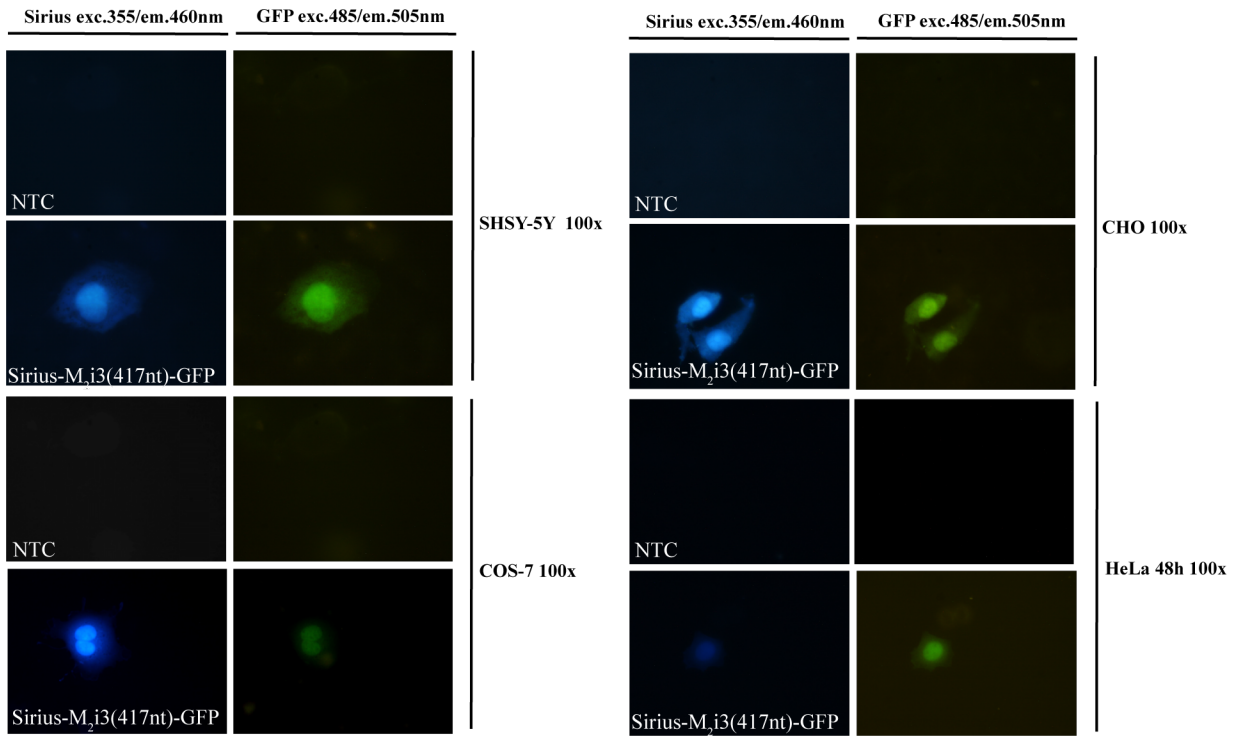

Supp. Fig. 4. Expression of the bicistronic plasmid Sirius-M_2i3(417n)-EGFP in four different cell lines

Expression of Sirius was driven by the canonical scanning mechanism of translation initiation, while EGFP expression was driven by an IRES dependent mechanism. All Sirius-M_2i3(417n)-EGFP transfected cells expressed both the Sirius

and EGFP proteins. On average, 25 ± 4% of the COS-7 cells transfected with Sirius-M_2i3(417n)-EGFP plasmid were blue fluorescence positive, while 17 ± 2% were green fluorescent positive, with only a few cells being only green.

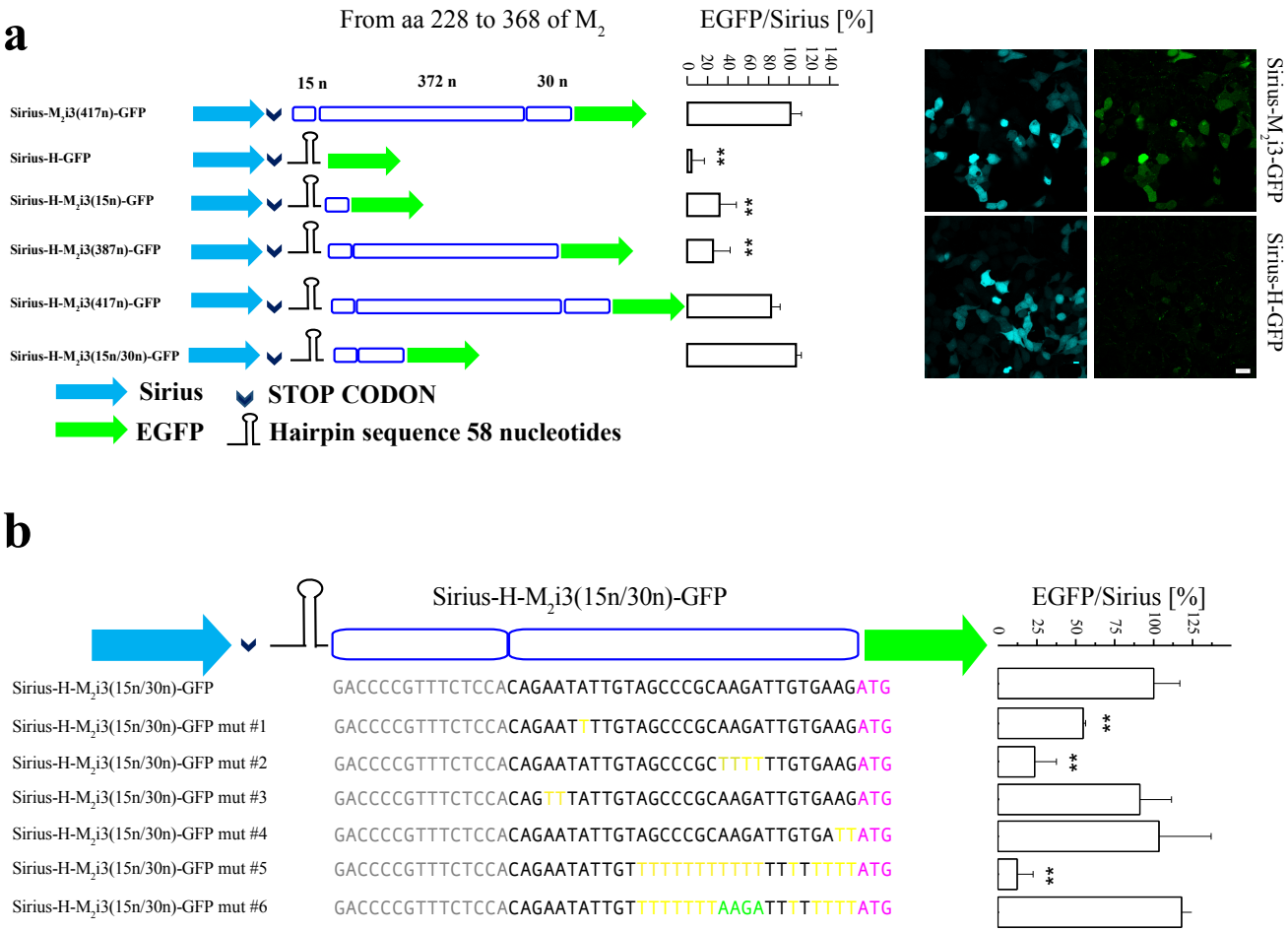

Fig. 3. Fluorescence assay of cap-independent translation of EGFP driven by the i3 loop mutants of the muscarinic M_2 receptor. a, left Schematic representation of bicistronic plasmids bearing the M_2 i3 loop between the coding regions of the Sirius and EGFP fluorescent proteins. A guanine nucleotide was originally inserted before the EGFP in the plasmid Sirius-H-EGFP in order to maintain in frame the sequences of the two fluorescent proteins. In all the other plasmids the sequence of the two fluorescent proteins is not in frame. Fifteen nucleotides derived from the M_2 i3 loop were inserted between the end of Sirius and the hairpin loop, in order to allow the easy scanning of the ribosome across the stop codon. **right**, Relative fluorescence of EGFP compared to Sirius, highlighting the efficiency of cap-independent translation for the control Sirius-M_3i3(417n)-EGFP and the six mutants. The insert shows the difference in the green fluorescence between two of the mutants. **b**, **left** Mutations of the bicistronic Sirius-H-M_2i3(15n/30n)-EGFP plasmids in the region of the M_2 i3 loop from nucleotides 1972 to 2001, in yellow are the modified nucleotides. In Sirius-H-M_2i3(15n/30n)mut#6-EGFP the four nucleotides in green (AAGA) were reinserted in the stretch of 20 T of Sirius-H-M_2i3(15n/30n)mut#5-EGFP. **right** Relative fluorescence of EGFP compared to Sirius, highlighting the efficiency of cap-independent translation for the control Sirius-H-M_2i3(15n/30n)-EGFP and the six mutants illustrated. Significance ($p < 0.01$) was calculated in **a** against Sirius-M_2i3(417n)-EGFP and in **b** against Sirius-H- M_2i3(15n/30n)-EGFP. Error bars are s.e.m.

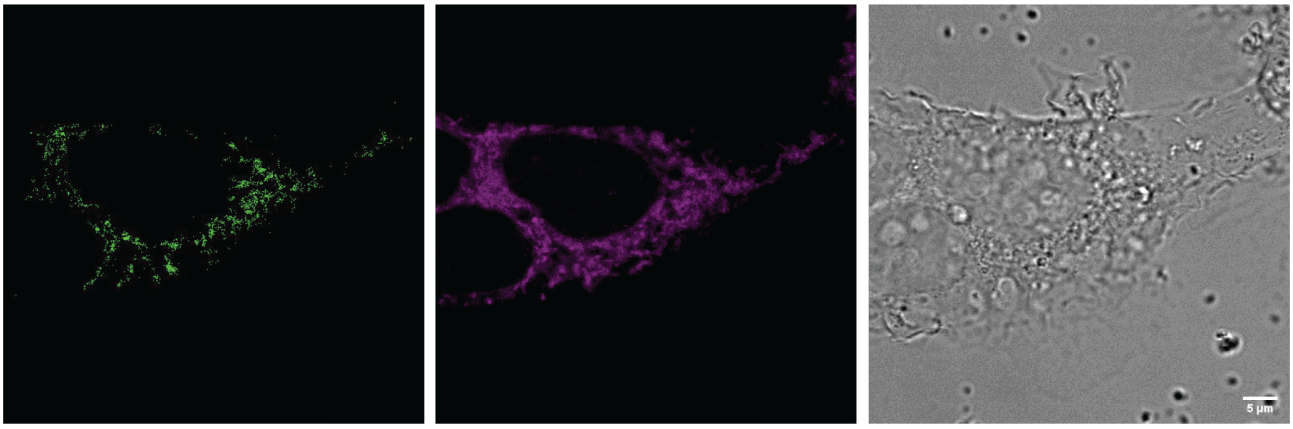

Supp. Fig. 5. Expression of the construct M_2-Hairpin-EGFP in HEK293 cells. (left) Confocal images of M_2-Hairpin-EGFP, (middle) Mitotracker Deep red staining, (right) DIC. Scale bar 5 µm.

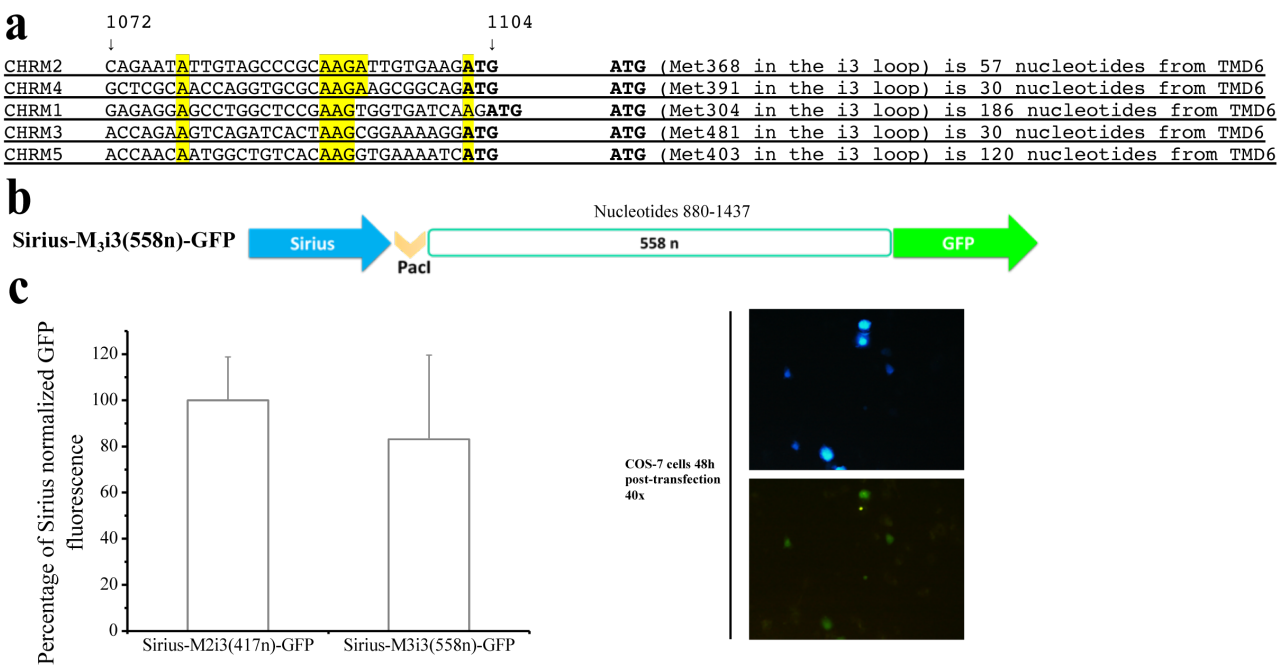

Supp. Fig. 6. Alignment of the nucleotide sequence 1072-1104 of the M_2 i3 loop with analogous sequences of the other four muscarinic receptors, and expression of the bicistronic plasmid Sirius-M_3i3(558n)-EGFP. a, The criteria for the alignment are described in the supplementary data. In yellow are highlighted the conserved nucleotides. In bold are the in frame ATG codons. Next to each sequence is indicated the codon number of the in-frame ATG and its distance in nucleotides from the beginning of TMDVI. **b,** Schematic representation of the bicistronic plasmid bearing the i3 loop of the rat muscarinic M_3 receptor (558 nucleotides from nucleotide 880 to nucleotide 1437) between the coding regions of the Sirius and EGFP fluorescent proteins. **c**, EGFP expression in COS-7 cells transfected with the bicistronic plasmid Sirius-M_3i3(558n)-EGFP.

662 **Supplementary Table 2. Radioligand binding and activation properties of M_3 receptor mutants.** Binding
663 characteristics and stimulation of phosphatidylinositol accumulation by M_3, M_3stop273 and the co-transfected M_3trunk(1-
664 272) and M_3tail(M-388-586). Untransfected COS-7 cells did not show any [^{3}H]NMS specific binding. N.B. = no specific
665 [^{3}H]NMS binding.

Binding data				Phosphatidylinositol accumulation assay	
Receptor	Bmax (fmol/mg)	[^{3}H]NMS KD (pM)	Carbachol IC50 (μM)	Carbachol EC50 (μM)	Maximum increase in IP_1 level above baseline (%)
M_3	1120 ± 71	29 ± 2	59 ± 4	4.2 ± 0.5	183 ± 15
M_3trunk(1-272)+ M_3tail(388-589)	114 ± 17	23 ± 2	48 ± 5	1.4 ± 0.1	126 ± 12
M_3stop 273	52.3 ± 0.5	31.3 ± 2.8	56 ± 2	1.1 ± 0.1	89 ± 13

666

667 **Supp. Table 3. Ligand binding of M_3 receptor mutants with single and double stop codons.** Number of [^{3}H]NMS
668 binding sites in COS-7 cells transiently transfected with the indicated M_3 receptor mutants with single and double stop
669 codons.

Receptor	Bmax (fmol/mg)	Receptor	Bmax (fmol/mg)
M_3stop273	54 ± 1	M_3stop273/stop503	N.B.
M_3stop240	N.B.	M_3stop273/stop503 + M_3tail(388-589)	120± 15
M_3stop503	N.B.	M_3stop240/stop503+ M_3trunk(1-272)	N.B.
M_3stop240+ M_3trunk(1-272)	44 ± 3	M_3stop240/stop503+ M_3tail(388-589)	N.B.
M_3stop503+ M_3tail(388-589)	135 ± 12	M_3stop273/fr.sh.	120 ± 4
M_3stop240/stop503	N.B.	M_3stop273/Hairpin	30 ± 2

670

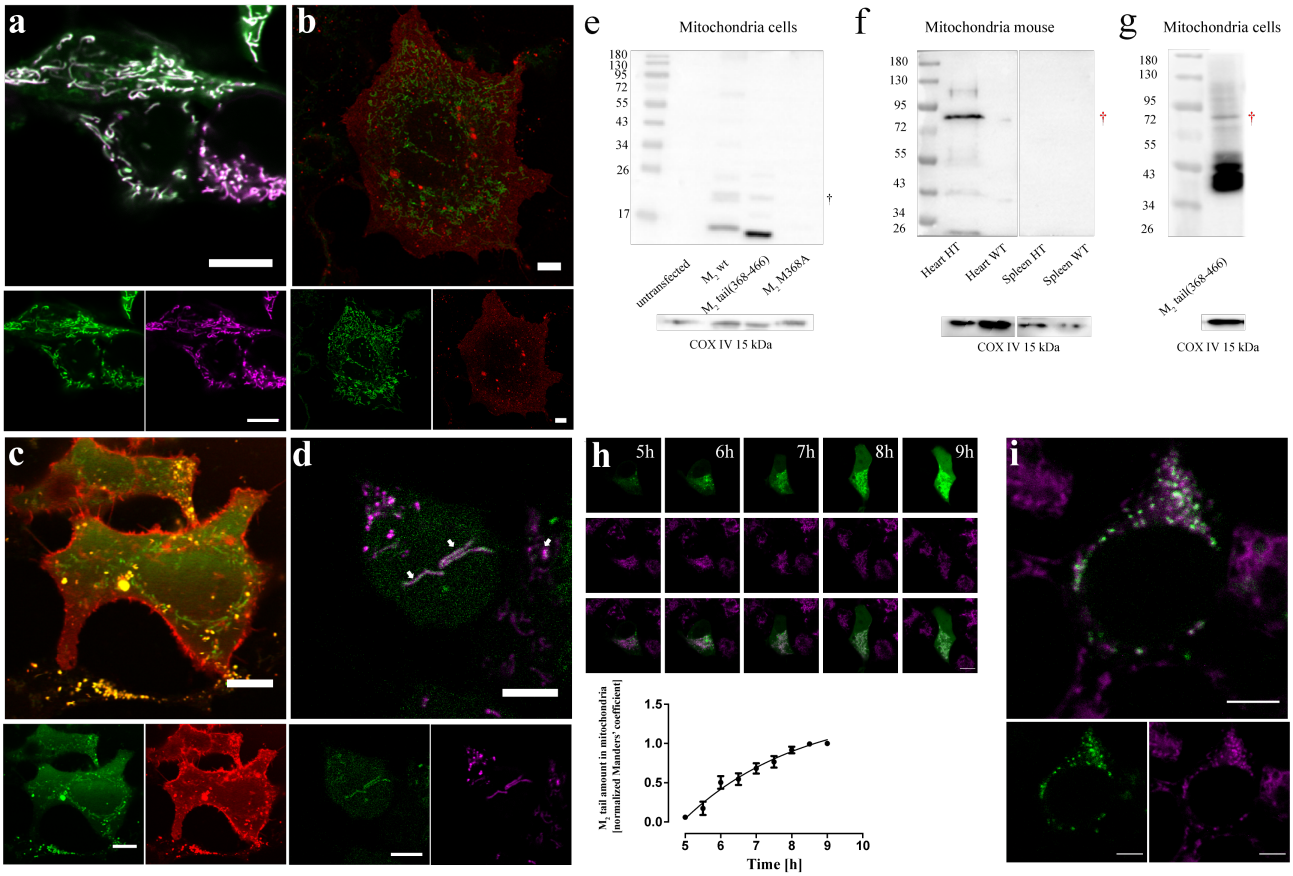

Fig. 4. Localization of fluorescently labeled M_2 mutant constructs: microscopy and western blots analysis. a, Colocalization of M_2tail(368-466)-EGFP (green) together with the mitochondrial targeted dye Mitotracker (magenta) in HEK293 cells. Separate spectral channels are displayed below. **b**, Co-expression of M_2tail(368-466)-EGFP (green) and wild type M_2-mRuby2 (red) in HEK293 cells. Separate spectral channels are displayed below. **c**, Cellular localization of the construct M_2-mRuby2-STOP-M_2-i3-tail-EGFP in HEK293 cells. Expression of the M_2tail(368-466)-EGFP (green) after the STOP codon is an indicator of the endogenous IRES activity. While M_2-mRuby2 localizes correctly and predominantly to the cell plasma membrane, M_2tail(368-466)-EGFP localizes in the cytosol as well as, strongly, to the cell mitochondria. Separate spectral channels are displayed below. **d**, M_2-fr.sh.-EGFP (green) expressed in conjunction with Mitotracker (magenta). The EGFP is expressed despite the creation of an in-frame stop after M368, confirming endogenous cap-independent translation of the M_2tail(368-466). Arrows indicate areas of colocalization with the mitochondria. Separate spectral channels are displayed below. **e**, Western blot (10% TRIS-Glycine PAA gel) of mitochondria purified from Hek293 cells transfected with the M_2-Myc, M_2tail(368-466)-Myc, M_2M368A-Myc, together with an untransfected control are blotted using an anti-myc antibody. Loading control was verified by immunoblotting COXIV. **f**, Western blot (8% TRIS-Glycine PAA gel) of mitochondria purified from tissue preparations originating from the indicated organs of M_2-tdtomato knock-in mice (HT) and wild-type animals (WT), detected using an anti-tdtomato antibody. Please note that the band at 80kDa is aspecific, and is more prominent in the WT lane due to higher loading. **g**, Western blot (8% TRIS-Glycine PAA gel) of mitochondria purified from HEK293 cells transfected with the M_2tail(368-466)-tdtomato, together with an untransfected control. Mitochondrial proteins were blotted using an anti-tdtomato antibody. Loading control was verified by detecting the 15 kDa mitochondrial matrix protein Cox-IV. **h** Time course of M_2tail(368-466)-EGFP import in the mitochondria of a HEK293 cell over a 4h interval, starting 5h after cell transfection, as indicated. Panels, from top to bottom show M_2tail(368-466)-EGFP (green), Mitotracker (magenta) and overlay displaying increasing colocalization over time. Chart at the bottom quantifies colocalization of the M_2tail(368-466)-EGFP

in the mitochondria by calculating the Manders Coefficients (n=7 cells, from 3 independent transfections, error bars are s.e.m.) (See **Methods**). **i**, Detail of a HEK293 cell expressing the M_2-GFP11 construct together with pmito-GFP1-10. The M_2-GFP11 was sequentially transfected 24 h after the pmito-GFP1-10 (see **Methods**) Magenta overlay indicates mitotracker. White signal in the overlay indicates M_2tail(368-466) trafficking to the organelle. All confocal micrographs were obtained by sequential imaging using 488 nm excitation and detection in the 520-600 nm (EGFP), 561 nm excitation and detection in the 580-650 nm (mRuby2) and at 633 nm and detected in the 650-700 nm range (Mitotracker) using HyD detectors in Photon Counting Mode. Scale bars are 10 µm throughout.

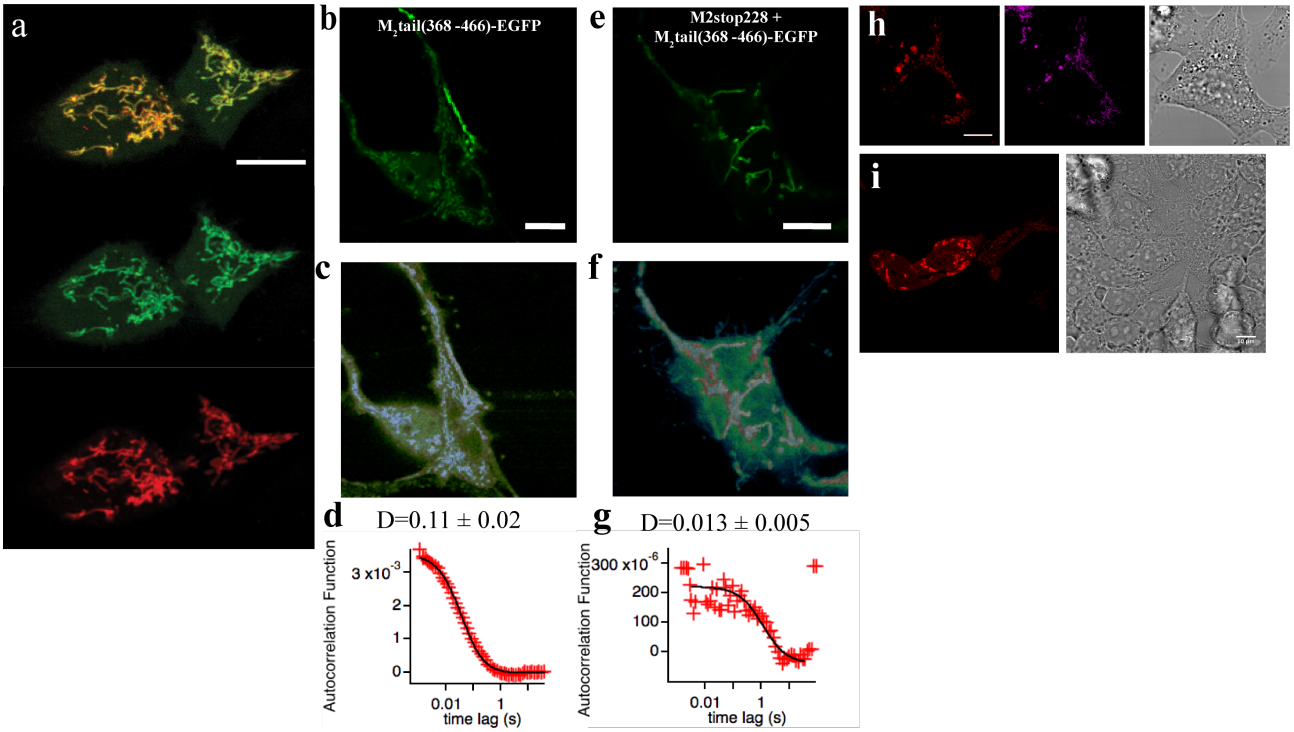

Supp. Fig. 7. Subcellular localization of the M2tail(368-466). a, Confocal image displaying the colocalization (top) of M2tail(368-466)-EGFP (green, middle)) in HEK293 cells, co-expressed with the outer mitochondrial membrane marker Tom20-mCherry (red, bottom). **b** expression of M2tail-EGFP displaying marked mitochondria and cytosolic localization. **c**, Glasbey colorscale representation of panel (**b**) highlighting the low-intensity pixels. **d**, autocorrelation function of the M_2tail(368-466)-EGFP diffusion taken at or in proximity of the basal membrane, yielding a mean diffusion coefficient of 0.11 $\mu m^2/s$, incompatible with membrane diffusion. **e**, co-expression of M_2stop228 and M_2tail(368-466)-EGFP. M_2stop228 is unlabeled. M_2tail(368-466)-EGFP maintains the localization to the mitochondria observed in cells expressing M_2tail(368-466)-EGFP alone, but it is also localized to the plasma membrane, visible in panel **f**, Glasbey colorscale representation of panel **e** highlighting the low-intensity pixels. **g**, autocorrelation function of the M_2tail(368-466)-EGFP diffusion taken at or in proximity of the basal membrane, yielding a mean diffusion coefficient of 0.013 $\mu m^2/s$, compatible with membrane diffusion. **h**, Cellular localization of M_2tail-mRuby2, together with Mitotracker deep red staining of the mitochondrial network and corresponding DIC image. **i,** Cellular localization of M_2tail-tdtomato and corresponding DIC image. All panels originate from Laser Scanning Confocal Microscope sequential acquisitions, with laser lines 488 nm (EGFP) 561 nm (mRuby2 and tdtomato) and 633 nm (Mitotracker deep red), and corresponding emission filters in the ranges 520-600 nm, 570-620 nm and 640-750 nm. Scale bars 10 µm.

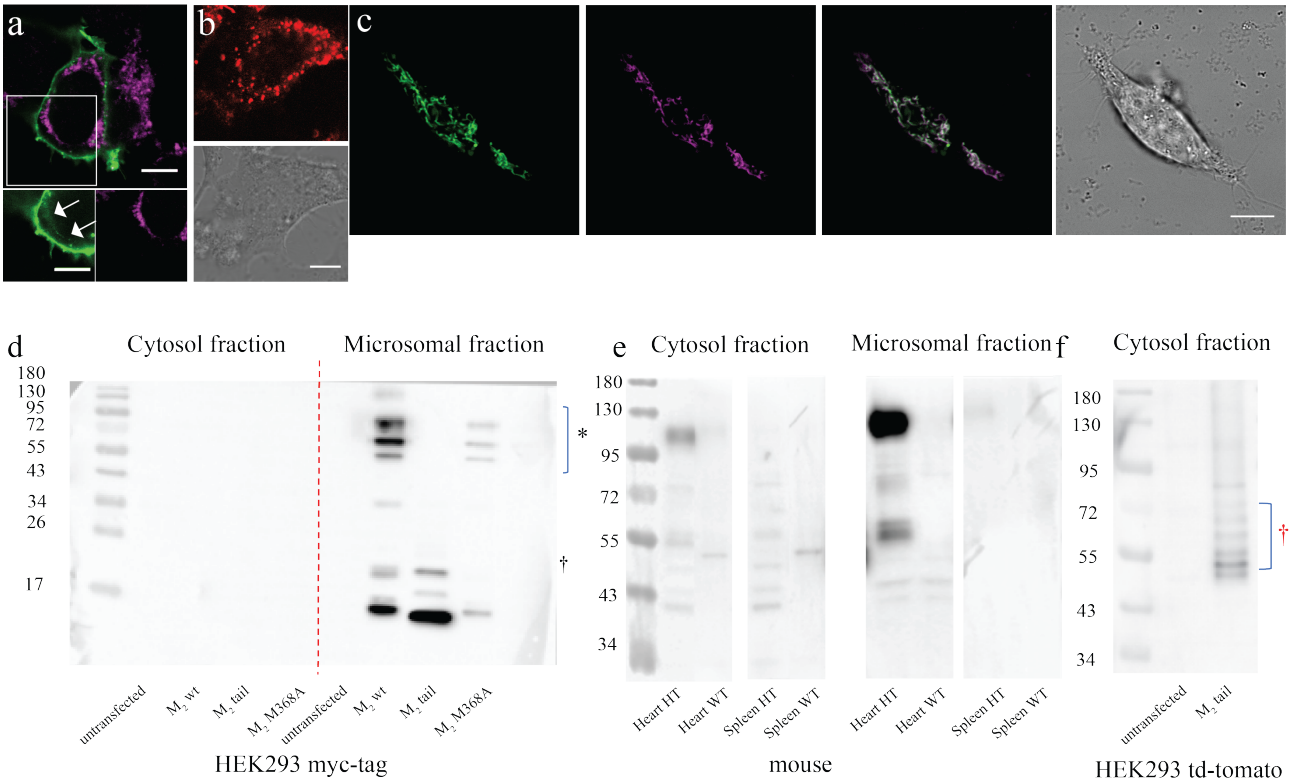

717

718 **Supp. Fig. 8. Mitochondrial localization of the M2tail fragment**. **a**, Confocal image of M_2-EGFP (green) expressed in
719 conjunction with Mitotracker (magenta) in HEK293 cells. Separate panels below. **b,** Confocal image of HEK293 cell
720 expressing *M_2fr.sh-mRuby2*, together with DIC, below. **c**, Confocal sequential images displaying the localization of
721 fluorescently labeled M_2tail(368-466)-EGFP (green), together with the mitochondrial network (magenta), colocalization
722 (white) and DIC image in COS-7 cells. Scale bars are 10 µm. Confocal sequential acquisitions were performed with 488
723 nm excitation and 520-600 nm detection (EGFP), and with 561nm excitation and 600-750 nm detection (mCherry) and
724 633 nm excitation and 650-750 nm detection (Mitotracker) using HyD detectors in Photon Counting Mode. **d,** Western
725 blot (10% TRIS-Glycine PAA gel) of the cytosolic and microsomal fractions resulting from the mitochondria purification
726 of lysates of HEK293 transfected with myc-tagged constructs, as displayed in **Fig. 4e**. **e**, Western blot (8% TRIS-Glycine
727 PAA gel) of the cytosolic fraction resulting from the mitochondria purification of lysates of HT and WT tissues of a
728 tdtomato transgene mice, as displayed in **Fig. 4f.** **f**, Western blot (10% TRIS-Glycine PAA gel) of the cytosolic fraction
729 resulting from the mitochondria purification of lysates of HEK293 transfected with M_2tail(368-466)-tdtomato, as
730 displayed in **Fig. 4g**.

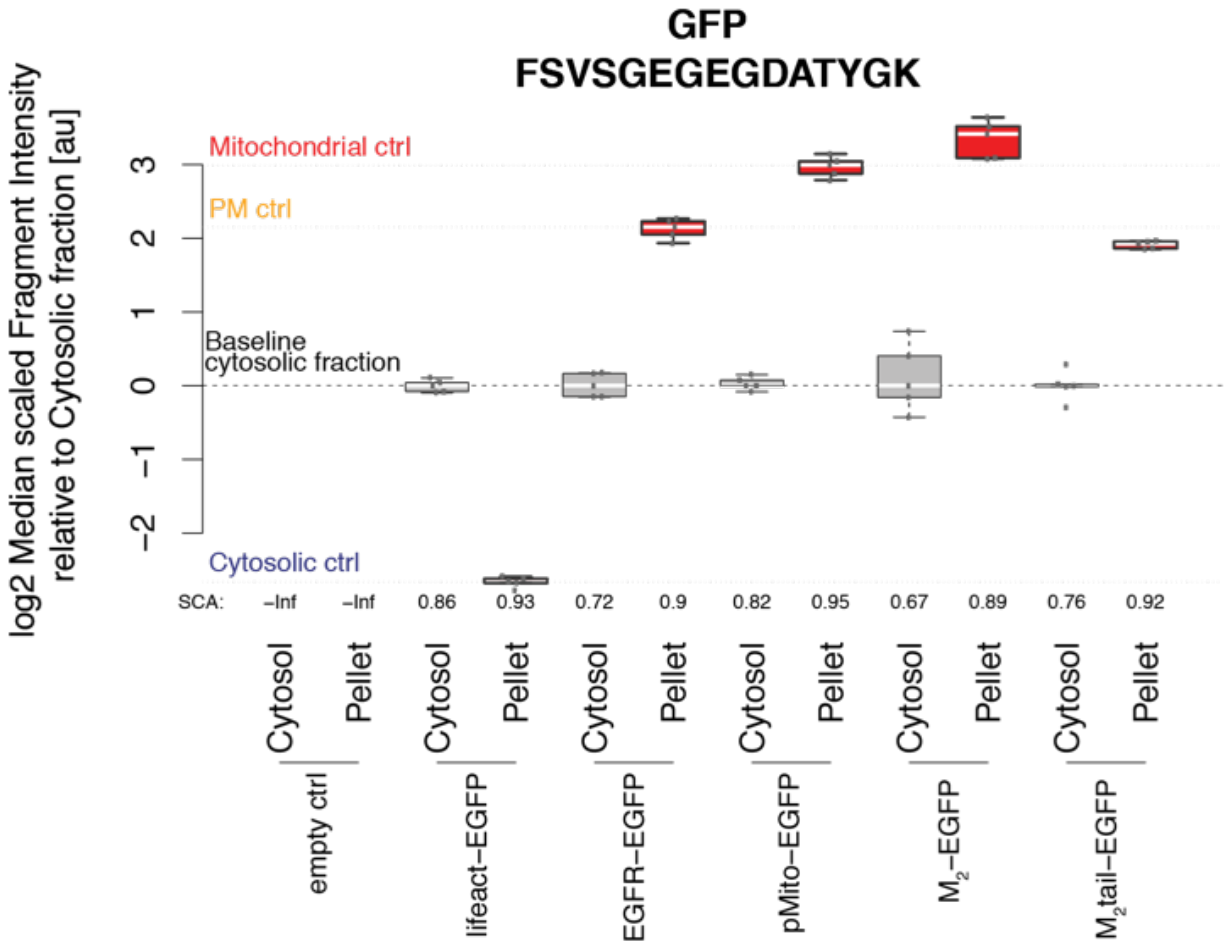

Supp. Fig. 9 Relative abundance estimates of EGFP and M_2 receptor from PRM based mass spectrometric measurements. Normalized fragment intensities were calculated for the peptide FSVSGEGEGDATYGK (specific for EGFP) for cytosolic and pellet fractions and for different constructs. Each preparation was normalized relative to the cytosolic fraction, if data was available. Median levels of cytosolic, plasma membrane and mitochondrial control markers are shown in the left panel. For each identified peptide the normalized spectrum contrast angle, indicating the similarity of the recorded spectrum to the reference spectrum, is indicated below each plot.

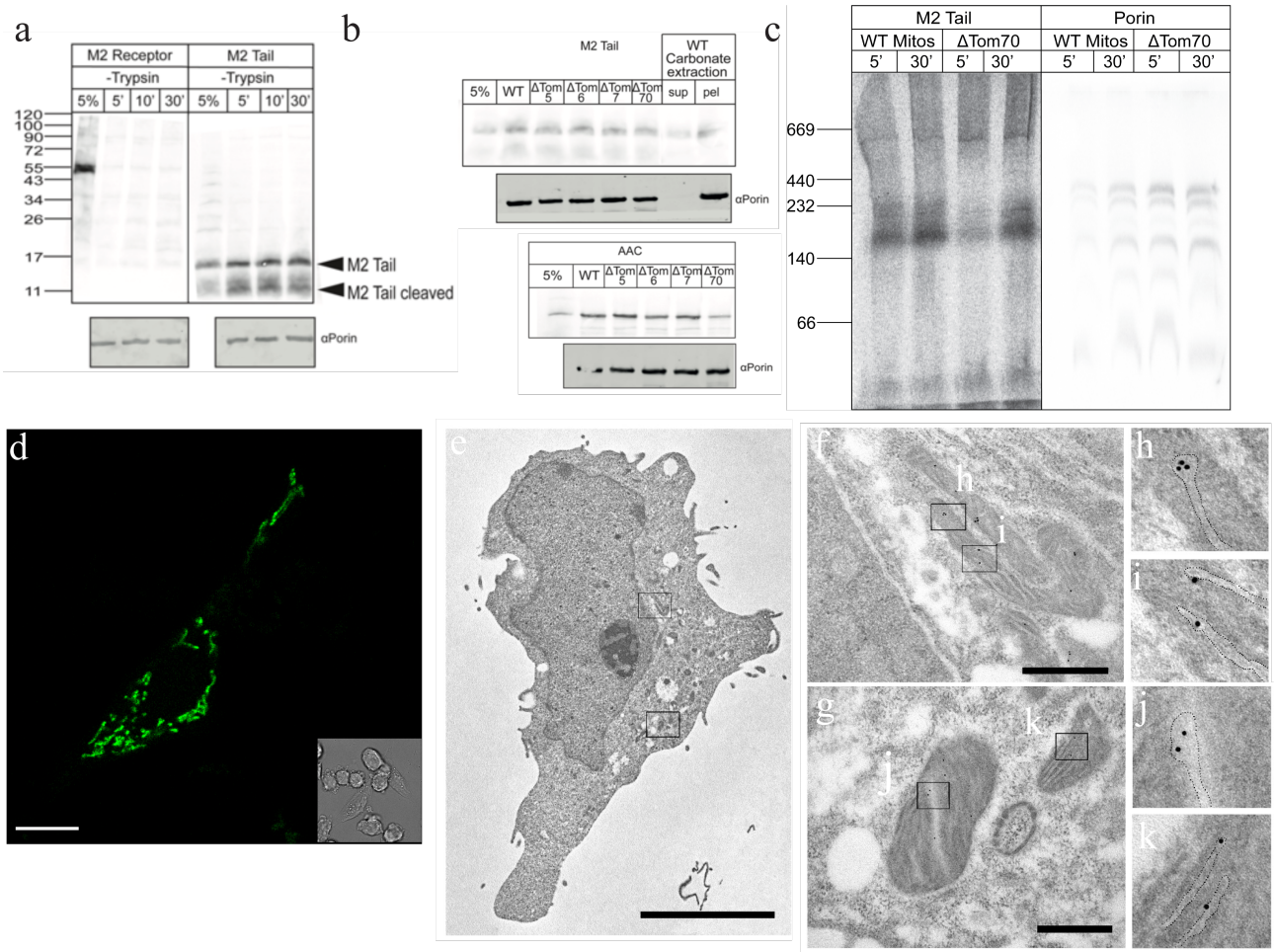

Supp. Fig. 10. In vitro mitochondrial import of M_2tail(368-466) and electron microscopy of M_2stop228. a, Import of M2-tail fragment in yeast mitochondria: 35S-labelled and translated in-vitro full length muscarinic M_2 receptor or M_2tail(368-466) expressing 5 C-terminal Methionines were incubated with isolated yeast mitochondria for various timepoints in the presence of the inner membrane potential (**See Supplementary Methods**). Samples were then washed in breaking buffer and loaded onto a 12% Tris-Tricine gel followed by semi-dry transfer and visualized via a phosphorimager. 5% of the crude protein was loaded as a control (left lane). To test for equal mitochondrial loading, αPorin was probed via western blot. The kinetics pattern of M_2tail is what it is expected for a protein imported in mitochondria: the appearance of the cleaved M_2-tail is indicative of a processing of the fragment once imported in mitochondria. **b,** ^{35}S-labelled M_2tail(368-466) or AAC (an integral internal mitochondrial membrane protein) were imported into isolated yeast mitochondria originating from different knock-out lines for outer membrane transporters (ΔTom). Samples were incubated for 30 minutes, and then washed in breaking buffer. After import, 100 µg of mitochondria were subject to Carbonate extraction to determine if M_2tail(368-466) is integrated into a lipid bilayer (Pellet) or loosely associated/soluble (Supernatant). Samples were then loaded onto a 12% Tris-Tricine gel followed by semi-dry transfer and visualized via a phosphorimager. To test for equal mitochondrial loading anti-αPorin was used via western blot. **c,** ^{35}S-labelled M_2tail(368-466) and αPorin were imported into isolated wild-type or ΔTom70 mitochondria for the indicated timepoints. Samples were then washed in breaking buffer and loaded on blue-native page followed by gel drying and visualized via a phosphorimager. **d,** Confocal images displaying the mitochondrial localization of M_2tail-GFP11 + M_2tail-GFP1-10, with corresponding DIC image. **e**, TEM micrograph of a COS-7 cell showing a large nucleus, several mitochondria and vacuoles nearby. Bar: 5 µm. **f-g**, High magnification of portion of the cell cytoplasm showing a few

gold particles confined to the mitochondria. Bar: 500 nm. **h-k,** Gold particles appear associated with the mitochondrial cristae, highlighted by the dotted line. A total number of 236 gold particles in 40 mitochondria from 19 sections were detected.

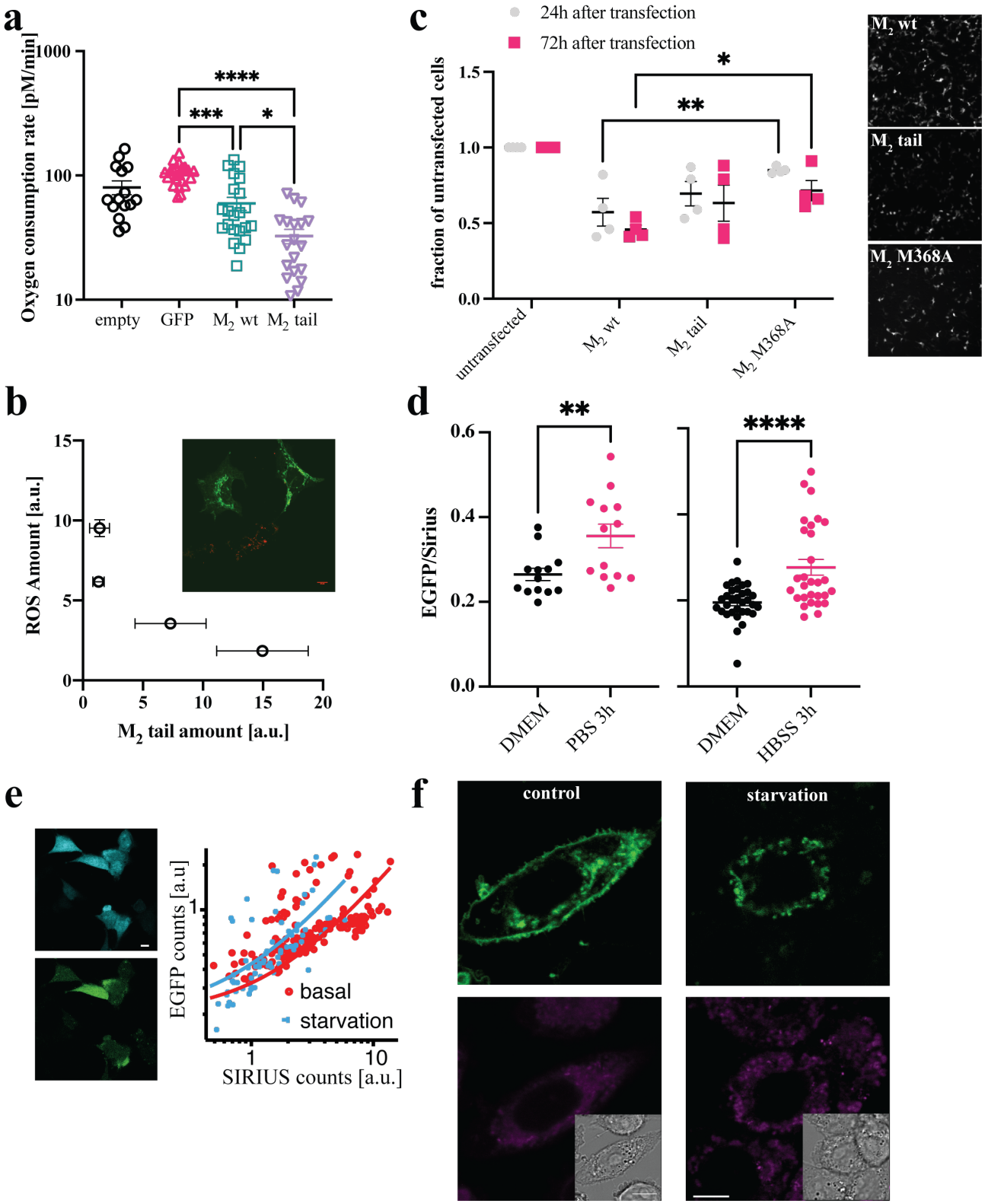

Fig. 5. Effects of M_2 mutants on mitochondrial function and cell metabolism in transfected HEK293 cells. a, Basal oxygen consumption upon HEK293 cell stress -following starvation- measured by a Seahorse assay at a constant temperature of 37 °C. **b**, Localization of M_2tail(368-466)-EGFP in HEK293 (green) cells stained with a marker for reactive oxygen species (Cell Rox Deep Red, ThermoFisher). Relationship between green (M_2tail abundance) vs red (amount of ROS produced) fluorescence intensities measured from regions of the mitochondrial network. The data were binned in four groups as a function of the amplitude of Cell Rox Deep Red signal (0-2.5, 2.5-5. 5-7.5 and 7.5-10 intensity counts). **c**, Cell viability assay performed on HEK293 cells transfected with M_2, M_2tail(368-466) and M_2(M368A), compared to an untransfected control. Cells were counted 24h and 72h after transfection in T-25 flasks, exposed throughout to 100 nM atropine. The experiments were performed in two biological replicates, each with two technical replicates. Transfection efficiency (to the right of the chart) was monitored thanks to the mRuby2 fluorescent reporter within a bicistronic cassette within each vector (see **Methods**). **d**, 96-well plate reader measurement of the increase of EGFP fluorescence relative to Sirius in COS-7 cells transfected with the bicistronic Sirius-M_2i3(417n)-EGFP plasmid and starved for three hours respectively in PBS (left panel) (n= 3 transfections, 16 wells) and HBSS (right panel) (n=1 transfection, 16 wells). **e,** Representative single cell confocal and DIC micrographs of HEK293 cells expressing the Sirius-M_2i3(417n)-EGFP construct in basal conditions, together with scatter plot of the average EGFP and Sirius fluorescence intensity values measured from single cells in basal (red dots) and 3h HBSS starvation (blue dots) conditions. **f**, HEK293 cells were sequentially transfected with pMito-GFP1-10 (24h) and M_2-GFP11 (8h, of which 6h under starvation conditions). (left panels) HEK293 cells grown in full culture medium and (right panels) HEK293 cells starved for 6 h after transfection of M_2-GFP11.Shown are EGFP fluorescence (top, with DIC inset) and Mitotracker (bottom).

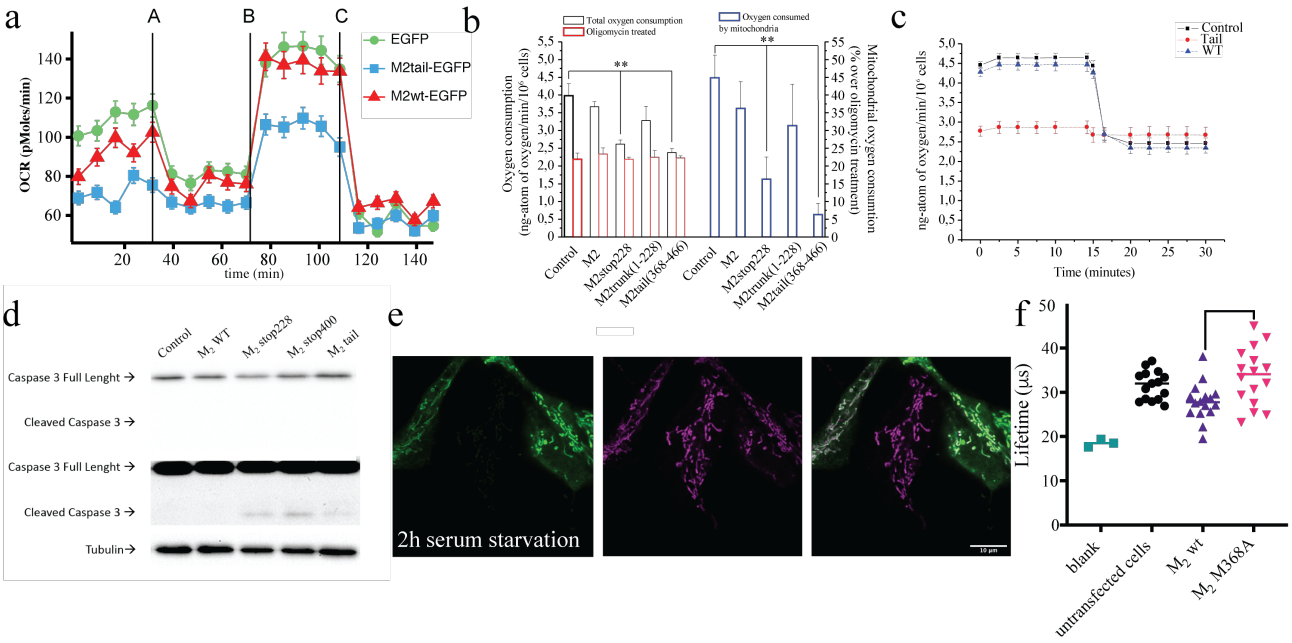

Supp. Fig. 11. Supplemental data on the effect of the M_2tail(368-466) fragment on mitochondrial function and cell metabolism. a, Representative experiment of Seahorse assay showing the time course of oxygen consumption inhibition by M_2tail(368-466)-EGFP and wild type M_2-EGFP, compared to the same experiments performed in control cells transfected with EGFP. The rate of ATP-linked respiration measured after oligomycin administration is decreased in M_2tail and slightly decreased in M_2 cells as well as compared to the controls. FCCP, an ionophore, was added to each cell type to investigate the cellular bioenergetic reserves that seem to be slightly reduced only in the M_2 tail cells. **b**, Oxygen consumption measured by a Clark type electrode-based-polarographic method at a constant temperature of 37 °C. After

790 15 minutes of basal respiration, the ATP synthase inhibitor oligomycin was added at a concentration of 17 nM. Oxygen
791 consumption in the absence and presence of oligomycin is represented by black and red bars, respectively. The blue bars
792 represent the percentage of mitochondrial oxygen consumption (total minus oligomycin treated) in cells transfected with
793 each construct. **c**, is a representative experiment showing the time course of inhibition of oxygen consumption by
794 M_2tail(368-466), compared to the same experiments performed in control cells and cells transfected with the M_2 wild type
795 construct, upon addition of oligomycin. Results are given as ng-atom of oxygen/min/10^6 cells. **d**, Western blot of caspase-
796 3 cleavage in COS-7 cells transfected with the indicated M_2 receptor mutants 48h after transfection (top panel, normal
797 contrast; bottom panel, increased contrast). **e,** Confocal sequential images of M_2tail(368-466)-EGFP (green), Mitotracker
798 (magenta) and overlay upon 2h of serum starvation. Scale Bars are 10 µm. **f**, Extracellular oxygen consumption assay of
799 HEK293 cells transfected with the indicated M_2 receptor mutants using a fluorogenic dye quenched by Oxygen. Blank
800 indicates the dye lifetime measured in wells containing the dye, but no cells.

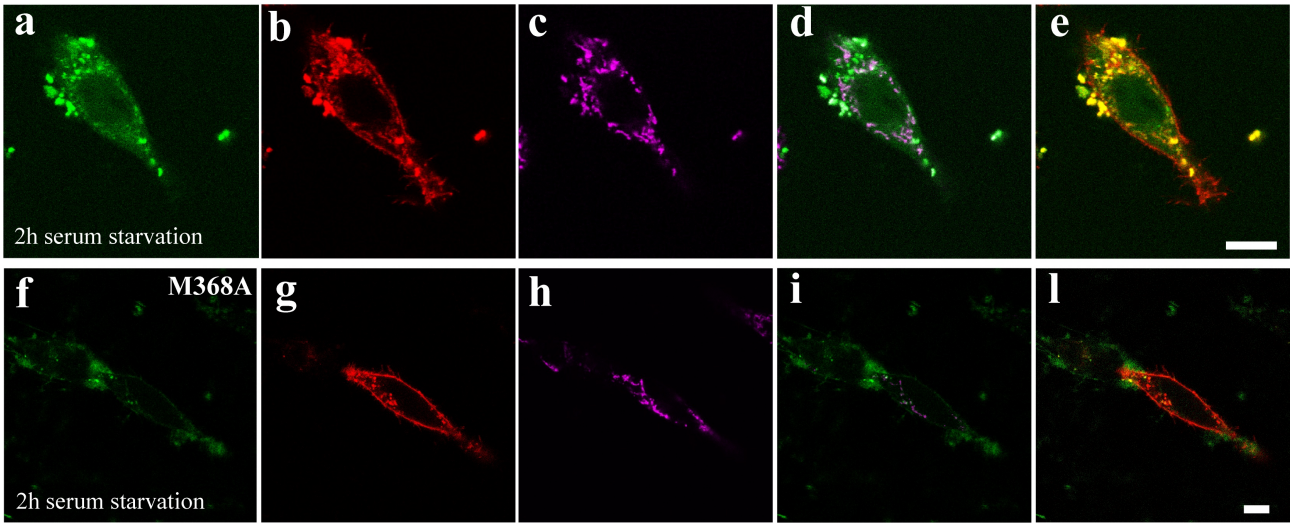

801

802 **Supp. Fig. 12. Functional aspects of mitochondrial localization of the M_2tail(368-466) fragment. a-e**, Mitochondrial
803 localization of the IRES mediated C-terminal fragment is enhanced upon cellular stress. HEK293 cells transfected with
804 the super construct M_2-mRuby2-STOP-M_2-i3-tail-EGFP display increased localization of the EGFP labelled portion to
805 the mitochondria, upon serum starvation for 2 hours and incubation of the cells in HBSS buffer, in presence of
806 Mitotracker: **a**, is IRES-driven M_2tail(368-466)-EGFP. **b,** Cap dependent M_2-mRuby2 + IRES-driven M_2tail(368-466)-
807 mRuby2, both derived from the M_2-mRuby2 gene. **c**, Mitotracker Deep Red **d**, Overlay of Mitotracker Deep Red and
808 EGFP channel. **e**, Overlay between GFP and mRuby2. **f-l**, Localization of the mutant construct M_2(M368A)-mRuby2-
809 STOP-M_2-i3-tail-EGFP in HEK293 cells after 2 hours incubation in HBSS buffer. The same legend as in **a-e** applies.
810 Bottom: Schematic structure of the mega constructs M_2(M368A)-mRuby2-STOP-M_2-i3-tail-EGFP. This construct is
811 similar to the M_2-mRuby2-STOP-M_2-i3-tail-EGFP construct but the methionine 368 in the M_2 sequence has been replaced
812 with alanine. The asterisks represent the stop codons at the end of mRuby2 and EGFP. EGFP was excited at 488 nm and
813 fluorescence collected between 500-600 nm; mRuby2 was excited at 561 nm and fluorescence collected between 580-

620 nm. Mitotracker deep red was excited at 633 nm and fluorescence collected between 650-750 nm. Scale bars are 10 µm.

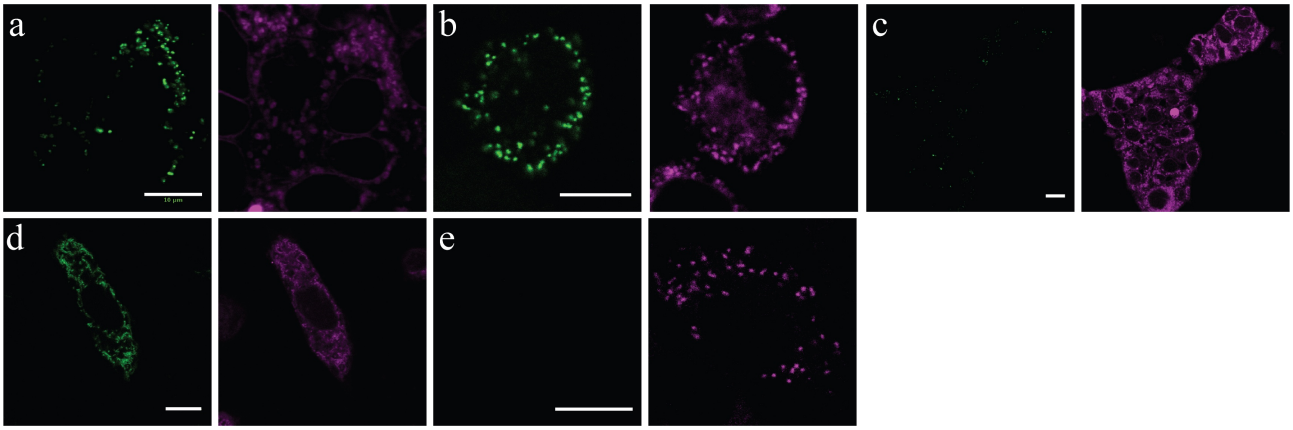

Supp. Fig. 13. Cellular localization of split GFP constructs in HEK293 cells. Confocal micrographs of **a,** co-expression of SMAC-GFP11 and SMAC-GFP1-10 (positive control) and corresponding Mitotracker deep red image. **b,** mito-GFP11 and mito-GFP1-10 (positive control). **c,** M_2tail(368-466)-GFP11 and SMAC-GFP1-10. **d,** M_2tail(368-466)-GFP11 and mito-GFP1-10. **e,** mito-GFP1-10 alone (negative control). EGFP (green) was excited at 488 nm and fluorescence collected between 500-600 nm. Mitotracker deep red (magenta) was excited at 633 nm and fluorescence collected between 650-750 nm. Scale bars are 10 µm.

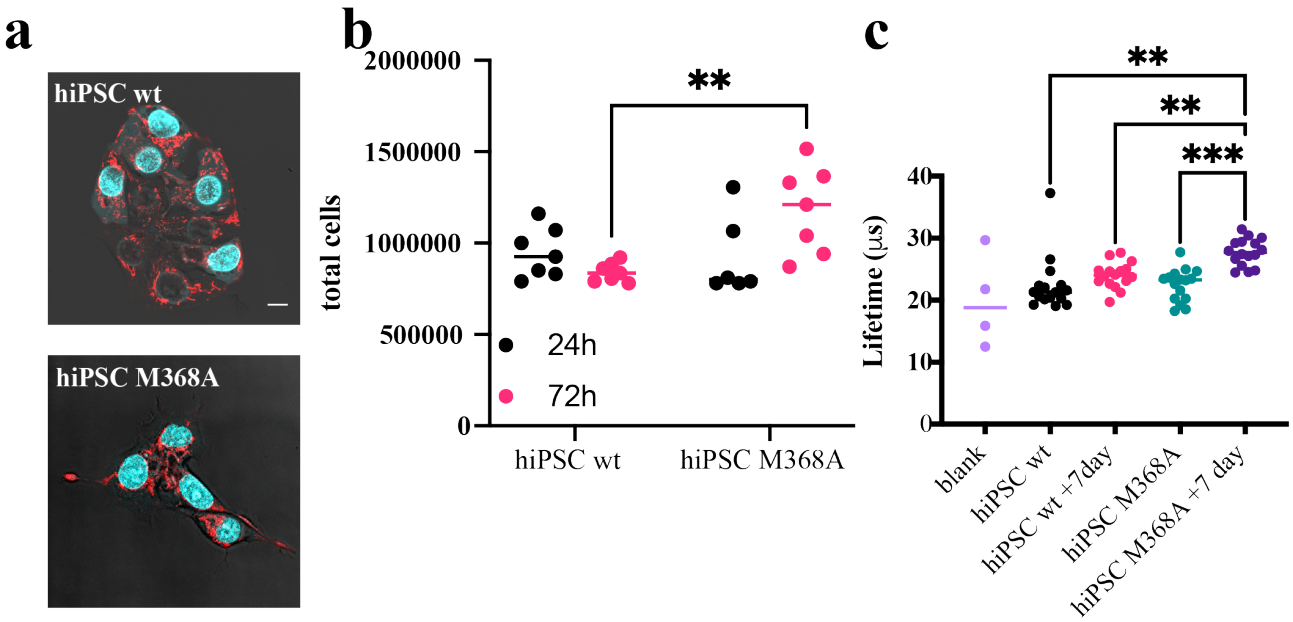

Fig. 6. Effects of M368A mutation on cell metabolism in hiPSCs a, Confocal micrographs of wt hiPSCs (left) and those harboring the M368A mutation within the M_2 gene (right), stained with DAPI (cyan) and Mitotracker (red). **b**, Cell proliferation assay performed for wt hiPSCs and M368A hiPSCs grown in T25 flasks. Cells were counted 24h and 72h after seeding. **c**, Extracellular oxygen consumption assay, performed on wt and M368A hiPSCs, prior to and after 7 days

undirected differentiation. The lifetime of a commercial dye increases as oxygen in the medium is progressively consumed by the cells. The data displayed are collected after 60 minutes incubation.

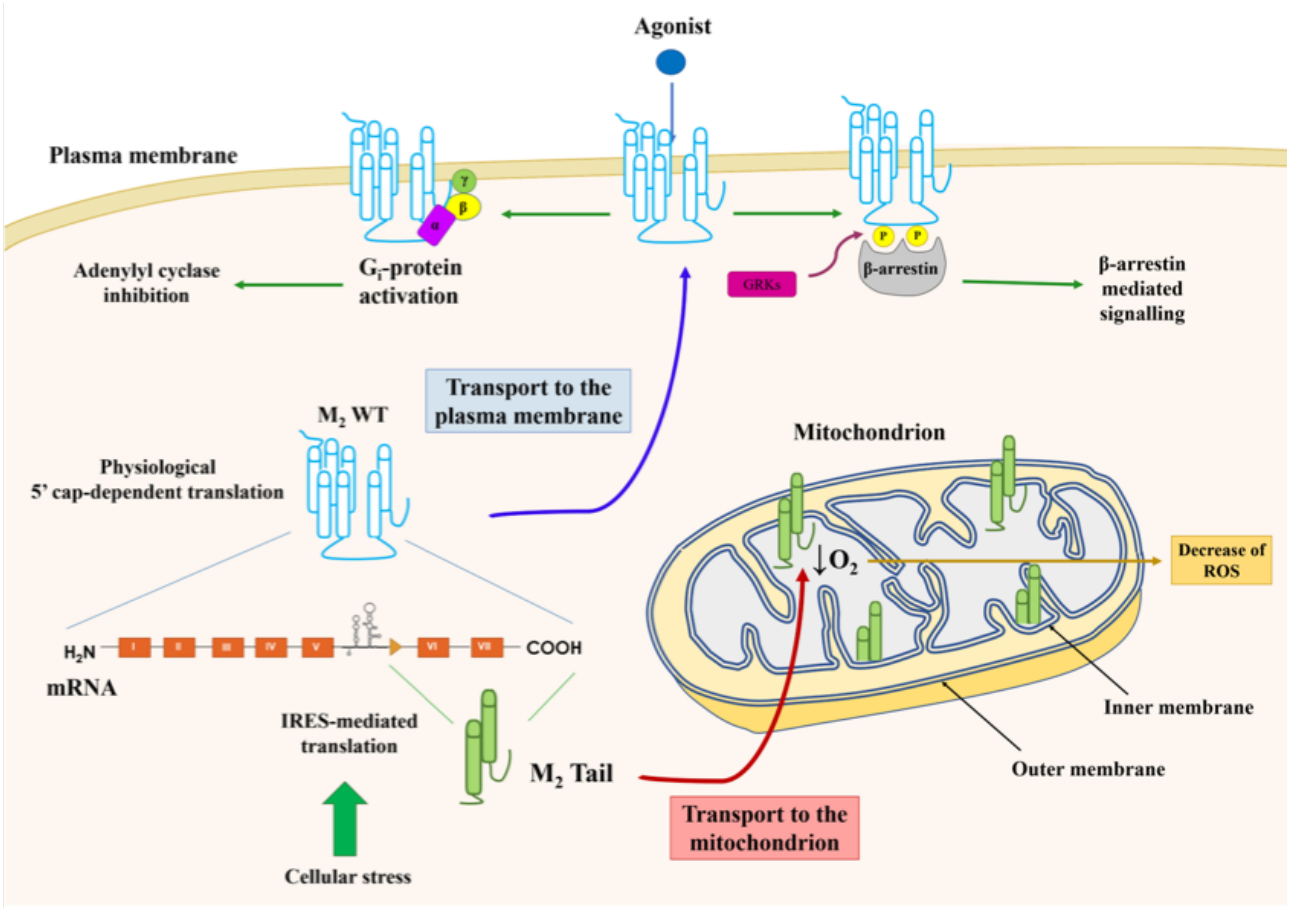

Fig. 7. Schematic representation of the wild type M_2 receptor gene products, their destination in the cell and their function. The M_2 receptor gene give rise to two different transcripts: when translation starts from the canonical cap site the wild type M_2 receptor is generated (in blue). When translation is driven by the internal ribosome entry site (IRES) the C-terminal fragment M_2tail is generated (in green). The two proteins are then sorted in two different cell compartments where they play completely different roles: the M_2 receptor is transported to the plasma membrane where it functions as a G protein-coupled neurotransmitter receptor and inhibits the adenylyl cyclase and β-arrestin mediated signalling. The M_2tail is instead transported in the mitochondria where it inhibits mitochondrial respiration and reduces ROS formation. IRES driven M_2tail translation is probably stimulated in para-physiological and pathological conditions and might have a protective role in cells expressing muscarinic M_2 receptors.

841 # Methods

842 **Statistical analysis.** Significance values reported in the graphs, in comparing tabulated values, were
843 determined by a one-tailed Student t-test using Prism 9 (GraphPad Software), and significance values
844 (p-values) are indicated according to the following legend: **** $p<0.0001$; *** $0.0001<p<0.001$; **
845 $0.001<p<0.01$; * $0.01<p<0.05$. p-values larger than 0.05 are deemed non-significant. Unless otherwise
846 indicated, bar charts and scatter plots indicate average value with s.e.m.

847

848 **Generation of mutant muscarinic M_2 receptors**. Multiple receptor mutants were constructed starting
849 from the human M_2 muscarinic receptor expressed in the pcD vector [36]. The constructs are sketched in
850 **Supplementary Fig. 1**. The two expression plasmids referred as M_2trunk(1-283) (containing
851 transmembrane domains I-V and the N-terminal portion of the third cytoplasmic loop) and M_2tail(281-
852 466) (containing transmembrane domains VI and VII, and the C-terminal portion of the third
853 cytoplasmic loop) were described previously [12].

854 *M_2stop228* – This plasmid was created by substituting codon 228 (CAA) with a stop codon (TAA) at
855 the N-terminal of the i3 loop of the wild type M_2 receptor.

856 *M_2stop228/stop400* – This plasmid was created by inserting an additional stop codon – TGG was
857 substituted with TAA – at the position codon 400 of the TM region VI of the M_2stop228
858 mutant.

859 *M_2stop400* – This plasmid was created by substituting codon 400 (TGG) with a stop codon (TAA) in
860 the TM region VI of the wild type M_2 receptor.

861 *M_2stop196* – This plasmid was created by substituting codon 196 (TAT) with a stop codon (TAA) in the
862 TM region V of the wild type M_2 receptor.

863 *M_2stop196/stop400* – This plasmid was created by inserting an additional stop codon in the TM region
864 VI of the M_2stop196 mutant, where TGG was substituted with TAA at position of the
865 codon 400.

866 *M_2stop228/fr.sh.* – This plasmid was created by inserting four bases (AATT) fifteen nucleotides
867 downstream of the stop codon to create a shift in the correct reading frame of the
868 M_2stop228 mutant.

869 *M_2stop228/hairpin* – This construct was created by inserting a 42 bases long sequence
870 (AGGGGCGCGTGGTGGCGGCTGCAGCCGCCACCACGCGCCCC). fifteen
871 nucleotides downstream of the stop codon of the M_2stop228 mutant. Upon transcription,
872 this palindromic sequence has been shown to form a hairpin structure with a ΔG value
873 of −64 kcal/mol that blocks effectively ribosome scanning [37,38].
874 *M_2stop228/stop248, M_2stop228/stop296 and M_2stop228/stop368* – These three constructs were obtained
875 by substituting the three in-frame ATG codons (1. ATG 248, 2. ATG 296 and 3. ATG
876 368) with the stop codon TAA downstream of the stop228 of the M_2stop228 mutant.
877 *M_2trunk(1-228)* – This plasmid was created by substituting codon 228 (CAA) with a stop codon (TAA)
878 at the N-terminal of the i3 loop of the wild type M_2 receptor followed by removal of the
879 downstream sequence.
880 *M_2tail(368-466)* – This construct was created by removing all bases of the M_2 receptor sequence up to
881 codon 368 (ATG) of the C-terminal of the i3 loop. The resulting plasmid encodes for a
882 polypeptide fragment that contains the trans-membrane domains VI and VII along with
883 the C-terminal portion of the third cytoplasmic loop.
884 *M2(M368A)* – In this construct the third in-frame methionine of the i3-loop of the M_2 muscarinic
885 receptor (ATG) was mutated to alanine (GCG).
886 *M_2-Myc, M_2stop228-Myc, M_2stopM368A-Myc, M_2tail(368-466)-Myc and M_2stop40-Myc* – M_2-Myc was
887 purchased from OriGene. This plasmid encodes the human M_2 receptor with a Myc (
888 tag at the C-terminus of the protein. M_2stop228-Myc was obtained by replacing the 0.9
889 Kb BmtI-PspOMI fragment of the M_2stop228 mutant with the corresponding fragment
890 of M_2-Myc. M_2stop400-Myc was obtained by substituting the codon 400 (TGG) with a
891 stop codon (TAA) of the M_2-Myc. All the constructs have an additional DDK tag after
892 the C-Myc. Subsequently, all C-Myc constructs were extracted by PCR and subcloned
893 into a bicistrionic pVitro2-MCS plasmid (Invivogen), allowing for the expression of a
894 reporter gene (in our case the red fluorescent protein mRuby2) after an IRES sequence,
895 in order to check for transfection efficiency.
896

897 **Generation of bicistronic constructs expressing Sirius and EGFP proteins (Fig. 3a).**

898 *Sirius[PacI-M_2i3(685-1101)]EGFP* – This bicistronic construct was created by inserting the i3 loop of
899 the muscarinic M_2 receptor, from nucleotide 685 to nucleotide 1101, between the
900 ultramarine fluorescent protein (Sirius) and the green fluorescent protein (EGFP). Eight
901 nucleotides corresponding to the recognition site of the PacI enzyme were inserted
902 between Sirius and the i3 loop of the wild type M_2 receptor to alter the reading frame
903 downstream of the Sirius stop codon. Hereafter this plasmid is referred to as Sirius-
904 M_2i3(417n)-EGFP.

905 *Sirius[PacI-M_2i3(685-699)-Hairpin-G]EGFP* – This bicistronic construct was created by inserting a 42
906 nucleotides hairpin loop (see above) between Sirius and the EGFP fluorescent protein.
907 The hairpin loop was spaced from the Sirius stop codon by inserting a PacI recognition
908 sequence and 15 nucleotides of the M_2 i3 loop sequence comprised between nucleotide
909 685 and nucleotide 699. A G nucleotide was also inserted following the 42 nucleotides
910 of the hairpin loop and upstream of the initial ATG triplet of the EGFP to restore a
911 correct reading frame. Throughout the text we referred to this plasmid as Sirius-H-
912 EGFP.

913 *Sirius[PacI-M_2i3(685-699)-Hairpin-G-PacI-M_2i3(685-1101)]EGFP* – This bicistronic construct was
914 created by adding 417 nucleotides of the i3 loop of M_2 from nucleotide 685 to nucleotide
915 1101 to the plasmid *Sirius[PacI-M_2i3(685-699)-Hairpin-G]EGFP*. An additional PacI
916 restriction site was also inserted upstream of this segment of the i3 loop. Throughout
917 the text we referred to this plasmid as Sirius-H-M_2i3(417n)-EGFP.

918 *Sirius[PacI-M_2i3(685-699)-Hairpin-G-PacI-M_2i3(685-699/1072-1101)]EGFP* – This bicistronic
919 construct was created by deleting from the plasmid *Sirius[PacI-M_2i3(685-699)-Hirpin-*
920 *G-PacI-M_2i3(685-1101)]EGFP* 372 nucleotides of the M_2 i3 loop, from nucleotide 700
921 to nucleotide 1071. Throughout the text we referred to this plasmid as Sirius-H-
922 M_2i3(15n/30n)-EGFP.

923 *Sirius[PacI-M_2i3(685-699)-Hirpin-G-PacI-M_2i3(685-699)]EGFP* – This bicistronic construct was
924 created by adding 15 nucleotides of the i3 loop of M_2 from nucleotide 685 to nucleotide

925 699 to the plasmid *Sirius[PacI-M_2i3(685-699)-Hirpin-G]EGFP*. An additional PacI
926 restriction site was also inserted upstream of this short segment of the i3 loop.
927 Throughout the text we will refer to this plasmid as Sirius-H-M_2i3(15n)-EGFP.
928 *Sirius[PacI-M_2i3(685-699)-Hirpin-G-PacI-M_2i3(685-1071)]EGFP* – This bicistronic construct was
929 created by adding 387 nucleotides of the i3 loop of M_2 form nucleotide 685 to nucleotide
930 1071 to the plasmid *Sirius[PacI-M_2i3(685-699)-Hirpin-G]EGFP*. An additional PacI
931 restriction site was also inserted upstream this long segment of the i3 loop. Throughout
932 the text we will refer to this plasmid as Sirius-H-M_2i3(387n)-EGFP.
933 *Mutants of the Sirius-H-M_2i3(15n/30n)-EGFP plasmid* – Based on the sequence alignment of amine and
934 adenosine GPCRs, several conserved nucleotides were mutated in order to define the
935 putative IRES sequence. These mutants are reported in **Fig. 3b**.
936 The fluorescence intensities of the two spectral bands were quantified by the use of a fluorometer and
937 the EGFP intensity values normalized to those of Sirius.
938
939 **Constructs for fluorescence microscopy.**
940 *M_2-EGFP* – The wild type M_2 muscarinic receptor was cloned into the pEGFP-N1 expression cassette,
941 between the restriction sites HindIII and XbaI.
942 *M_2-mRuby2* – The wild type M_2 muscarinic receptor was cloned into the mRuby2 vector (Addgene
943 plasmid #40260).
944 *M_2tail(368-466)-EGFP* – The M_2tail(368-466)-EGFP was constructed so that the receptor protein would
945 start from the third in-frame methionine of the M_2 i3 loop (M368). The EGFP gene was
946 fused C-terminally following a short restriction site sequence (TCTAGA) of the XbaI
947 enzyme.
948 *M_2tail(368-466)-mRuby2* – The M_2tail(368-466)-mRuby2 was constructed so that the receptor protein
949 would start from the third in-frame methionine of the M_2 i3 loop (M368). The mRuby2
950 gene was fused C-terminally following a short restriction site sequence (TCTAGA) of
951 the XbaI enzyme.

952 *M_2-mRuby2-STOP-M_2-i3-tail-EGFP* – This mega construct was obtained by fusing two preceding
953 constructs, M_2-mRuby2 and M_2tail(368-466)-EGFP, in a unique plasmid, but the M_2tail
954 started at codon 229 (M_2tail(229-466)-EGFP). After the stop codon of mRuby2 and
955 before the codon 229 of M_2tail was inserted a short restriction site sequence (TCCGGA)
956 of the BspEI enzyme (**Fig. 4**).

957 *M_2(M368A)-mRuby2-STOP-M_2-i3-tail-EGFP* – This mega construct is analogous to *M_2-mRuby2-STOP-*
958 *M_2-i3-tail-EGFP, but* the third in-frame methionine of the i3-loop of the M_2 muscarinic
959 receptor was mutated to alanine (M368A) (**Supplementary Fig. 1**).

960 *M_2fr.sh-EGFP* – A single base insertion (G) upstream of nucleotide 1102 of the wild type M2 receptor,
961 just before the third in-frame methionine of the i3-loop (M368), induces a frame shift
962 that, following 2 aminoacids, generates a stop codon (TAA) in the amino acid position
963 370 of the new reading frame. The construct is then fused to EGFP.

964 *M_2fr.sh-mRuby2* – As above, but the EGFP is replaced by a mRuby2.

965 *M_2-GFP11* – A short peptide 16 aminoacids long from the GFP protein, GFP11, was fused to the C-
966 terminus of the muscarinic M_2 receptor. GFP11 was custom syntethised and inserted as
967 a linker between the XbaI and XhoI restriction sites in the plasmid backbone of M_2-
968 EGFP.

969 *Mito*-GFP1-10 – The mitochondrial targeting sequence of the cytochrome c oxidase subunit 8A
970 (COX8A) was fused to the N-terminal of GFP1-10 fragment of GFP. GFP1-10 was
971 purchased from Addgene as Addgene plasmid 70219.

972 *Mito-GFP11* – The mitochondrial targeting sequence of COX8A was fused to GFP11 fragment. Mito
973 sequence was obtained from Addgene plasmid 23348.

974 *SMAC-GFP1-10* – The mitochondrial targeting sequence of the SMAC protein was fused to the N-
975 terminal of GFP1-10 fragment. SMAC was obtained from Addgene plasmid 40881.

976 *SMAC-GFP11* – The mitochondrial targeting sequence of the SMAC protein was fused to GFP11
977 fragment.

978 *M_2tail(368-466)-GFP1-10* – The GFP1-10 fragment was fused to the C-terminus of the muscarinic
979 M_2tail(368-466) receptor fragment.

980 *M_2tail(368-466)-GFP11* – The GFP11 fragment was fused to the C-terminus of the muscarinic
981 M_2tail(368-466) receptor fragment.
982
983 **Constructs for in-vitro mitochondrial import assays**
984 *PSP64-M_2tail(368-466)-5Met* - The vector backbone PSP64 (courtesy of Ruaridh Edwards). The
985 following primers: FWD: ATGATGTAAtctagaggaggcggacgc, REV:
986 CATCATCATccttgtagcgcctatgttcttataatg
987 were used to add five methionines to the C-terminal domain of the M_2tail(368-466)-
988 GFP11 template (see above) using Q5® Site-Directed Mutagenesis Kit (New England
989 Biolabs® Inc.). The construct was then extracted with appropriate restriction enzymes
990 (HindIII and XbaI) and ligated into the vector backbone PSP64 (courtesy of Ruaridh
991 Edwards).
992 *PSP64-M2R-5Met* – The following primers: FWD: ATGATGTAAtctagaggaggcggacgc REV:
993 CATCATCATccttgtagcgcctatgttcttataatg were used to add five methionines to the C-
994 terminal domain of to the M_2-GFP11 template (see above) using Q5® Site-Directed
995 Mutagenesis Kit (New England Biolabs® Inc.). The construct was then extracted with
996 appropriate restriction enzymes (HindIII and XbaI) and ligated into the vector backbone
997 PSP64.
998
999 All constructs were sequenced either with a Genetic Analyzer 3500 (Applied Biosystem®) or by a
1000 professional sequencing service (LGC Genomics, Berlin).
1001
1002 **Reverse transcription.** Reverse transcription was performed using a 24-nucleotide antisense oligo
1003 (TTACCTTGTAGCGCCTATGTTCTT) directed against the last 24 nucleotides at the 3' end of the M_2
1004 open reading frame. cDNA amplification was carried out with the same antisense oligo used for reverse
1005 transcription, together with a 24 nucleotides sense oligo (ATGAATAACTCAACAAACTCCTCT)
1006 directed against the first 24 nucleotides at the 5' end of the M_2 open reading frame.

1007 **Cell culture and transfection**. COS-7 (African green monkey kidney fibroblast-like SV40 transformed
1008 cell line) and CHO (Chinese Hamster Ovary) cells (from American Type Culture Collection) were
1009 grown at 5% CO_2 and 37 °C, in high glucose Dulbecco's modified Eagle's medium (DMEM)
1010 supplemented with 10% fetal bovine serum (FBS), 2 mM L-glutamine, 50 IU/ml penicillin, and 50
1011 mg/ml streptomycin, and non-essential amino acids. HeLa cells (from American Type Culture
1012 Collection) were cultured in the same medium, but with the double amount of L-glutamine. SHSY-5Y
1013 cells were cultured in Roswell Park Memorial Institute (RPMI) medium supplemented with 10% FBS,
1014 2 mM L-glutamine, 50 IU/ml penicillin, and 50 mg/ml streptomycin. Media and reagents used for cell
1015 cultures were from Euroclone, PAN Biotech, Biochrome and Sigma-Aldrich. Cell transfection was
1016 performed using FuGene® transfection reagents (Promega) as recommended by the manufacturer.
1017 Eighty percent confluent cells were washed twice with free-serum medium and the mix of FuGene and
1018 plasmid DNA was added. In every experimental condition 6-8 µg of plasmid DNA per Petri (10 cm^2)
1019 were used. Cells were grown for 48 h post-transfection before use. In co-transfection experiments, half
1020 amount of each plasmid DNA was used. All microscopy experiments were performed with transiently
1021 transfected HEK293 (Human Embryonic Kidney, ECACC 96121229 from Sigma-Aldrich Chemie
1022 GmbH) and COS-7 cells. HEK293 cells were cultured in DMEM (Dulbecco's modified Eagle's medium
1023 PAN biotech, Aidenbach, Germany), supplemented with 4.5 g/L Glucose, 2 mM L-Glutamine, 10%
1024 FCS, 100 units/mL penicillin and 0.1 mg/mL streptomycin and maintained at 37 °C and 5% CO_2. Cells
1025 cultured in 15-cm dishes were split at a 1:36 ratio into 6-well plates containing poly-D-lysine (PDL)-
1026 coated 24 mm glass coverslips. Cells were transfected using Effectene transfection reagent (QIAGEN)
1027 according to the manufacturer's instructions. Cells seeded on PDL-coated coverslips in 6-well plates
1028 were transfected 16 hours after seeding with 0.6 µg plasmid/well.
1029
1030 **Fluorescence microscopy**. Fluorescence microscopy experiments were performed either on a Leica
1031 SP5 (or SP8) Confocal Microscopes, using HyD photon counting detectors and an Argon/Ion laser (or
1032 white light laser) source for 488 nm/633 nm excitation and a solid-state diode laser (or white light laser)
1033 for 561 nm excitation. A solid-state diode laser was used for 405 nm excitation. A 40x 1.3 NA objective
1034 was used, and the electronic zoom was set to achieve a pixel size of 50 nm. For visualization,

1035 mitochondria of transfected cells were labelled for 30 minutes at 37 C with 50nM MitoTracker® Deep
1036 Red FM (Invitrogen™, Thermo Scientific).
1037
1038 **Ligand binding studies**. Cells were lysed 48 h post-transfection with ice-cold 2 mM EDTA, 1 nM Na-
1039 HEPES (pH 7.4), scraped with a rubber policeman in the presence of ~4 ml rinsing medium, and
1040 homogenized with a Polytron homogenizer (ULTRA-TURRAX) in binding assay buffer (50 mM Tris-
1041 HCl, pH 7.4, 155 mM NaCl, 0.01 mg/ml bovine serum albumin). Radioligand bindings were carried out
1042 at 37 °C for 3 h in a final volume of 1 ml. Non-specific binding was determined in presence of 1 μM
1043 atropine. For competition binding assays, increasing concentrations of carbachol (from 0.01 μM up to
1044 10 μM) were used in presence of 200 pM [^{3}H]N-Methylscopolamine ([^{3}H]NMS; 78.9 Ci/mmol;
1045 PerkinElmer).

1046 The bound ligand was separated from the unbound ligand using glass-fiber filters (Whatmann, GF/B)
1047 with a Brandel Cell Harvester, and filters were counted with a scintillation β-counter. K_D values of
1048 [^{3}H]NMS were calculated in direct saturation experiments, whereas carbachol Inibitory Concentration
1049 $(IC)_{50}$ values were calculated in competition curves, against 400 pM [^{3}H]NMS, fitted to one binding
1050 models using the iterative, non-linear least-squares regression analysis of OriginPro 7.5 software
1051 (OriginLab Corporation).

1052 **Phosphatidylinositol Breakdown Assay**. Transfected COS-7 cells were incubated with myo-
1053 [^{3}H]inositol (23 Ci/mmol; PerkinElmer) for 48 h. Immediately before the experiment the cells were
1054 washed twice with phosphate-buffered saline and incubated for 15 min in Eagle's medium containing
1055 10 mM LiCl and 20 mM HEPES. The medium was then replaced by 0.25 ml of the same medium
1056 containing the experimental agents. After a 1-hour incubation at 25 °C the reaction was arrested by the
1057 addition of 0.75 ml of 7.5% (w/v) ice-cold trichloroacetic acid followed by a 30-min incubation on ice.
1058 The trichloroacetic acid was extracted with water-saturated diethyl ether (3 × 4 ml), and levels of IP_1
1059 determined by anion exchange chromatography.
1060
1061 **Adenyl Cyclase Assay**. COS-7 cells were transfected with plasmid(s) containing the receptor of interest

1062 plus adenyl cyclase V. 24 h after transfection the cells were detached with trypsin and re-cultured in 24-
1063 well plates. Following an additional period of 24 h culture, they were assayed for adenyl cyclase activity.
1064 The assay was performed in triplicate**.** In brief, cells were incubated in 24-well plates for 2 h with 0.25
1065 ml/well of fresh growth medium containing 5 μCi/ml [^{3}H]adenine (PerkinElmer). The medium was then
1066 replaced with 0.5 ml/well of DMEM containing 20 mM HEPES, pH 7.4, 0.1 mg of bovine serum
1067 albumin, and the phosphodiesterase inhibitors 1-methyl-3-isobutylxanthine (0.5 mM) and Ro-20–1724
1068 (0.5 mM). AC activity was stimulated by the addition of 1 μM forskolin in the presence or absence of
1069 carbachol. After 10 min of incubation at +30 °C the medium was removed, and the reaction terminated
1070 by addition of perchloric acid containing 0.1 mM unlabeled cAMP followed by neutralization with
1071 KOH. The amount of [^{3}H]cAMP formed under these conditions was determined by a two-step column
1072 separation procedure (referenza?).
1073
1074 **Immunoblot of muscarinic M_2 receptor mutants transfected in HEK293 cells**. Cells were seeded in
1075 10 cm plates and transfected after 24h according to manufacturer protocols (Effectene, Qiagen) using 2
1076 μg of plasmid DNA. 48h after transfection cells were washed (2x) in ice cold PBS. 200 μL per plate of
1077 ice-cold lysis buffer were added. Lysis buffer was a RIPA buffer: 50 mM Tris-HCL pH 8, 150 mM
1078 NaCl, 1% TRITON, 0.5% sodium deoxycholate and 0.1% SDS. The following compounds were added
1079 to the buffer to a final 1x dilution: 100x Halt Protease Inhibitor Cocktail (Thermo Fisher), 100x 0.5 M
1080 EDTA and (10x) 10 mM PMSF. Cells were then scraped and the cell lysate transferred to pre-cooled
1081 1.5 mL Eppendorf tubes. The tubes were placed in a Thermomixer at 4 °C, 300 rpm for 30 minutes.
1082 Then the Eppendorf tubes were centrifuged for 30 minutes at 14000 rpm at 4 °C. The supernatant was
1083 then transferred to new Eppendorf tubes. Protein concentration in the cell lysates was quantified by a
1084 BCA assay (Pierce BCA Protein Assay Kit, from Thermo Fisher) according to manufacturer
1085 instructions.
1086 Cell lysates were loaded into 10% polyacrylamide gels. Cell lysates were loaded using Laemmli Buffer
1087 2x (Sigma Aldrich) in equal mass. As a reference marker we loaded 5 uL of PageRuler Prestained
1088 Protein Ladder (Thermo Fisher). Gels were mounted into a Mini Protean Tetra Cell kit (BioRad) using
1089 1x SDS running buffer. Gels were ran using a constant voltage of 90V for approximately 15 minutes,

1090 and afterwards at 130V for 45 minutes. Gels were transferred to PVDF membranes. Wet transfer was
1091 achieved by using the Mini Trans Blot Module (BioRad) in Wet Transfer Buffer (25 mM Tris pH 8.3,
1092 192 mM Glycine and 20% MetOH) at 350 mA for 90 minutes. The immunoblotted membranes were
1093 then blocked in 5% Milk in TBS-T for 1 hour at room temperature. The membrane was then incubated
1094 overnight at 4 °C with primary antibody solution using the following concentrations depending on the
1095 antibody used: 1:1000 anti **β**-actin (13E5) rabbit primary antibody (Cell Signaling), 1:1000 anti myc-
1096 Tag (9B11) mouse primary antibody (Cell Signaling). After overnight incubation, the membranes were
1097 washed 3x 10 minutes in TBS-T and incubated at RT for 1 h with a secondary antibody (1:10000 anti-
1098 mouse IgG/(anti rabbit) HRP-linked antibody from Cell Signaling).
1099 After the incubation with the secondary antibody, the membrane was washed 3x 10 minutes in TBS-T.
1100 Detection was achieved by eliciting HRP luminescence by incubating the membrane with SuperSignal
1101 WestFemto solution (Thermo Fisher) according to the manufacturer's instructions, and imaging the
1102 membrane using a c600 Transilluminator from Azure Biosystems.
1103
1104 **Animal Experiments.** All animal experiments were carried out according to the German animal welfare act,
1105 considering the guidelines of the National Institute of Health and the 2010/63/EU Directive of the European
1106 Parliament on the protection of animals used for scientific purposes. The animals had free access to food and
1107 water and were kept in individually ventilated cages under a 12h:12h light/dark regime (light from 6:30 am to
1108 6:30 pm), a constant 22±2°C temperature and 55±10% humidity.
1109 The transgenic line B6.Cg-Chrm2tm1.1Hze/J, also known as Chrm2-tdT-D knock-in, was obtained from 'The
1110 Jackson Laboratory' (Stock No: 030330). They are heterozygous animals, designed to have expression of a
1111 Chrm2/tdTomato fusion protein directed by the endogenous M2 muscarinic acetylcholine receptor
1112 promoter/enhancer sequences.
1113
1114 **Tissue preparation and immunoblot of endogenous M_2 receptor in Chrm2-tdT-D knock-in mice.**
1115 Mouse tissues were weighed out and ice-cold lysis buffer was added to approx. 0.2-0.5mg tissue/ml
1116 buffer (10mM K2HPO4, 150mM NaCl, 5mM EDTA, 5mM EGTA, 1% Triton X-100, 0.2% Na-
1117 deoxycholate. Fresh protease inhibitors PMSF 0.5mM, Na3VO4 0.1mM, NaF 50mM, Jenny's mix

1118 (Soybean trypsin inhibitor 3.2µg/ml, Aprotinin 2µg/ml, Benzamidin 0.5mM) were added to the buffer.
1119 Samples were first homogenized, and then pellet debris were centrifuged at 4°C for 30 minutes at max
1120 speed (tabletop) and the supernatant (soluble proteins) was transferred into fresh tube (pellets = non-
1121 soluble proteins)
1122 Protein concentration were determined with BCA assay. Cell lysates were loaded using Laemmli Buffer
1123 2x (Sigma Aldrich) in equal mass (see above for the immunoblot procedure) into 8% polyacrylamide
1124 gels.
1125 The membrane was then incubated overnight at 4 °C with primary antibody solution (1:1000 anti **β**-
1126 actin (13E5) rabbit primary antibody #4970 from Cell Signaling) (1:1000 anti GAPDH) (1:1000 anti-
1127 TdTomato rabbit primary antibody #632496 from Takara).
1128
1129 **Isolation of mitochondrial fractions and immunodetection.** Cells were seeded in 15 cm plates and
1130 transfected after 24h according to manufacturer protocols (Effectene, Qiagen) using 5 µg of plasmid
1131 DNA. 48h after transfection cells were harvested and centrifuged at 1000 rpm for 10 minutes,
1132 resuspended in NaCl 0.9% (w/v) and centrifuged at 1000 rpm for 10 minutes.
1133 Mouse tissue were freshly excised and placed in ice cold PBS (1x) . The samples were washed with
1134 NaCl 0.9% (w/v). The homogenization steps were performed with Precellys Evolution Homogenizer, at
1135 4500 rpm for 10 seconds.
1136 The samples were processed according to manufacturer protocols (Qproteome Mitochondria Isolation
1137 Kit, Qiagen). From the different steps were obtained three different fractions: the cytosolic, the
1138 microsomal and the mitochondrial fraction.
1139 The fresh mitochondrial pellet was resuspended in 150µL of ice-cold lysis buffer and the protein
1140 concentration of the three fractions from each sample was quantified with a BCA assay (see above).
1141 Cell lysates were loaded into 12% polyacrylamide gels using an SDS loading buffer (6x solution: 2.28g
1142 Tris-HCl, 2.313 DTT, 6g SDS, 30% Glycerol and 0.03% bromophenol blue in a final volume of 50 mL)
1143 in equal mass (see above for the immunoblot procedure).
1144 The membrane was then incubated overnight at 4 °C with primary antibody solution using the following
1145 concentrations: 1:1000 anti **β**-actin (13E5) rabbit primary antibody (#4970 from Cell Signaling), 1:1000

1146 anti-tdtomato rabbit primary antibody (#632496 from Takara), 1:1000 anti **β**-tubulin mouse primary
1147 antibody, 1:1000 anti GAPDH mouse primary antibody, 1:1000 anti COXIV mouse primary antibody
1148 (#ab33985 from abcam).
1149
1150 **Quantification of M_2tail(368-466) mitochondrial import kinetics from confocal time sequences.**
1151 Before imaging, 2.5×10^4 HEK-TSA cells were seeded in each PDL-coated well of the μ-Slide 8 well
1152 (Ibidi) with DMEM (ScienCell™) supplemented with 10% FBS and 1% P/S overnight, and transfected
1153 with a total of 2 μg C-terminal EGFP tagged M_2 tail using Lipofectamine 2000 (Thermo Fisher
1154 Scientific) according to the manufacturer protocol after washing with 200 μL PBS and refreshing with
1155 100 μL DMEM (ScienCell™) supplemented with 10% FBS and 1% P/S. After transfection for five
1156 hours, mitochondria of transfected cells were rapidly labelled with 50nM MitoTracker® Deep Red FM
1157 (Invitrogen™, Thermo Scientific) in FluoroBrite DMEM medium (Thermo Scientific) supplemented
1158 with 1% P/S for 20 minutes after the removal of old culture medium. After mitochondria labeling, the
1159 μ-Slide were washed twice with FluoroBrite DMEM medium (Thermo Scientific) and subsequently
1160 mounted onto the TCS SP8 confocal microscope (Leica) (See imaging). Firstly, the stage of the
1161 microscope was equilibrated in temperature, and the acquisition mode was set to the tile scanning. After
1162 storing the position of each desired transfected cells, the imaging mode was set to XYT and a HC PL
1163 APO CS2 40×/NA1.3 oil immersion objective was selected. Both DIC channel and HyD were utilized
1164 to obtain 512×512 pixels images. Laser wavelengths were set as described in the section Fluorescence
1165 Microscopy above. All settings remained the same throughout the whole measurement. Images were
1166 taken at every 30 minutes over a 5h interval. The images were afterwards analyzed by ImageJ software,
1167 using the Plugin 'JACoP'. Briefly, the degree of colocalization between EGFP-tagged M_2tail(368-466)
1168 (CH1) and MitoTracker stained mitochondria (CH2) was quantified by Mander's colocalization
1169 coefficients [39]. The two colocalization coefficients M1 ($M1 = \frac{CHB}{CH1}$) and M2 ($M2 = \frac{CHB}{CH2}$), CHB indicates
1170 overlapping pixels in channel 1 and channel 2. A threshold was determined for individual channel in
1171 order to distinguish specific signals from nonspecific ones. Due to their sensitivities to thresholds, the
1172 Pearson correlation coefficient (PCC)[40], as well as the faster decaying attribute of nonspecific signals,
1173 were also taken into account while estimating thresholds for each channel. For the analysis of each cell,

1174 the threshold for Mitotracker channel was kept constant. Whereas the threshold for EGFP channel was
1175 evaluated based on the PCC value.
1176
1177 **Transfection and expression of split-GFP constructs in HEK293 cells.** To perform the sequential
1178 split GFP complementation assay illustrated in **Figures 4h-i and 5f**, 3×10^5 HEK-TSA cells were seeded
1179 on a 10% poly-D-lysine (PDL)-coated 25mm coverslip in each well of a Falcon® 6-well flat-bottom
1180 plate (StemCell™) and cultured overnight. Cells were transfected using Effectene (see above) with a
1181 0.4 µg Mito-GFP1-10 plasmid. The cells were then washed once with fresh 2 mL phosphate-buffered
1182 saline (PBS) first and supplemented with 1.5 mL fresh DMEM medium (ScienCell™) supplemented
1183 with 10% FBS and 1% P/S. After adding the transfection mixture, the cells were cultured overnight.
1184 After the first transfection, a second transfection of a 0.6 µg plasmid encoding either the C-terminal
1185 GFP11 tagged M_2tail(368-466) or M_2 receptor was performed using the Effectene Transfection Reagent
1186 (Qiagen). After washing each well with 2 mL PBS, the old medium was exchanged with 1.5 mL low
1187 glucose Minimum Essential Medium (MEM) (Gibco™, Thermo Scientific) supplemented with 1% P/S,
1188 in order to create a stress-like cell starvation condition. After a four hours starvation, the cells were fixed
1189 using 4% polyformaldehyde (PFA)/PBS at 37°C for 30 minutes and washed twice with PBS before
1190 imaging.
1191
1192 **Oxygen consumption measured with the Seahorse assay.** $5x10^4$ COS7 cells were seeded in seahorse
1193 24MW plates with Complete media (DMEM supplemented with 10%FBS and 1X PS) and then
1194 incubated for about 4h at 37C in a cell incubator. After this incubation, cells were washed twice with
1195 Seahorse media supplemented with glutamate (1 mM), pyruvate (1 mM) and glucose (20 mM) and then
1196 incubated for 1h at 37 °C in an incubator without CO2 before being analyzed in the Seahorse XF
1197 Analyzers. In particular, the baseline cell oxygen consumption rate (OCR) was measured at the
1198 beginning of the assay, followed by measurements of ATP linked respiration and maximal respiratory
1199 capacity after the addition of respectively oligomycine (1 µM) and the FCCP protonophore (1 µM).
1200 Finally, rotenone (1 µM), an inhibitor of complex I, and antimycin (1 µM), inhibitor of complex III,

1201 were added to shut down completely the electron transport chain (ETC) function, revealing the non-
1202 mitochondrial respiration.
1203
1204 **Generation of M368A hiPSC clone.** The human induced pluripotent stem cell (hiPSC) line BIHi005-
1205 A (https://hpscreg.eu/cell-line/BIHi005-A) was used to generate an isogenic iPSC clone (BIHi005-A-
1206 39) with **M368A mutation** using a protocol previously described[41]. In brief, small guide RNA (sgRNA)
1207 targeting the M_2 gene close to the mutation site to be corrected were designed using the
1208 http://crispor.tefor.net/ webpage and the sgRNA (5`- AGTCATCTTCACAATCTTGC-3`) were
1209 synthesized by Integrated DNA technologies (https://eu.idtdna.com). The donor ssODN template was
1210 designed to convert the ATG to GCT and was synthesized as an Ultramar DNA oligo by IDT. (5´-
1211 AAAAGTGACTCATGTACCCCAACTAATACCACCGTGGAGGTAGTGGGGTCTTCAGGTCAG
1212 AATGGAGATGAAAAGCAGAATATTGTAGCCCGCAAGATTGTGAAGGCTACTAAGCAGCC
1213 TGCAAAA-3´). The Ribonucleoprotein (RNP) complexes were prepared by incubating of 1.5µg Cas-
1214 9 protein and 360 ng gRNA for 10 minutes at room temperature. For delivery of RNPs and ssODN
1215 template, 10µl cell suspension containing Cas9 RNPs and ssODN and 1x105 cells were electroporated
1216 using the Neon transfection System (ThermoFisher Scientific). The electroporated cells were plated in
1217 one well of 6 well plate with StemFlex media (ThermoFisher Scientific) supplemented CloneR™
1218 (Stemcell technologies). Three days after the transfection we analyzed the bulk population using the
1219 Sanger sequencing to estimate the editing efficiency. Thereafter, the automated single cell cloning of
1220 the genome edited cell pool was performed as described in protocol [42]. The clones were screened by
1221 SANGER sequencing. The positive confirmed clones were banked and characterized for pluripotency
1222 and karyotype stability as described in [43].
1223
1224 Briefly, for pluripotency assay, single cells were labelled with conjugated antibodies. Surface markers
1225 (SSEA1, SSEA4 and TRA1-60) staining was performed in unfixed cells by incubation with antibodies
1226 diluted in 0.5% BSA/PBS (10 min, 4 °C, dark). Intracellular markers (OCT3/4, NANOG) were stained
1227 by fixation/permeabilization solution (Miltenyi Biotec, 130-093-142) (30 min, 4 °C, dark) followed by

1228 antibody incubation in permeabilization buffer (Miltenyi Biotec) (30 min, 4 °C, dark). Analysis was
1229 done using the MACSQuant® AnalyzerVYB and FlowJo v10.4.
1230
1231 Briefly, for karyotype stability, genomic DNA was isolated using the DNeasy blood and tissue kit
1232 (Qiagen, Valencia, CA, United States) and samples were analyzed using the human Illumina OMNI-
1233 EXPRESS-8v1.6 BeadChip. First, the genotyping was analyzed using GenomeStudio 1 genotyping
1234 module (Illumina). Thereafter, KaryoStudio 1.3 (Illumina) was used to perform automatic normalization
1235 and to identify genomic aberrations utilizing settings to generate B-allele frequency and smoothened
1236 Log R ratio plots for detected regions. The stringency parameters used to detect copy number variations
1237 (CNVs) were set to 75 kb (loss), 100 kb (gain) and CN-LOH (loss of heterozygosity) regions larger than
1238 3 MB.
1239
1240 **Culture and handling of hiPSCs cells.** hiPSCs were cultured on Geltrex (Thermo Fisher) coated plates
1241 using: Essential 8 medium (Thermo Fisher). The culture was routinely monitored for mycoplasma
1242 contamination using a PCR assay. 10 µM ROCK Inhibitor Y-27632 2HCl (Selleck Chemicals, #SEL-
1243 S1049) was added after cell splitting to promote survival. hiPSC cultures were kept in a humidified
1244 atmosphere of 5% CO2 at 37°C and 5% oxygen. hiPSCs were undirectedly differentiated to a mixture
1245 of three lineages (ectodermal, endodermal and mesodermal) by replacing Essential 8 medium with
1246 DMEM-F12 medium supplemented with 10% FBS for seven days. 10 µM ROCK Inhibitor Y-27632
1247 2HCl (Selleck Chemicals) was added after cell splitting to promote survival.
1248
1249 **Cell proliferation assay with HEK293 cells.** $4x10^5$ HEK293 cells 24h after transfection and $4x10^5$
1250 hPSCs were seeded respectively in T25 flask and pre-coated T25 flask, in culture medium with Atropine
1251 at final concentration of 100nM; the medium with Atropine was replaced every day. After 72h from
1252 transfection of the HEK293 and from seeding of the hiPSCs, the medium and the cells were collected
1253 and centrifuged, the pellet was resuspended in the same amount of medium for each pellet; an aliquots
1254 of the resuspension was mixed with the same amount of Trypan blue (ratio 1:1), 10 microliters were
1255 used for counting in a Neubauer chamber.

1256

1257 **Fluorescence plate reader assays.** HEK293 cells were grown on 6 well plates without coverslips, and,
1258 upon reaching 60-70% confluence, the cells were transfected using Effectene (Quiagen, Venlo
1259 Netherlands) according to the manufacturer's instructions. After 24 h the cells were split and transferred
1260 to 96 well (black plate) at a seeding density of 50,000 cells/well. The 96 well plate was pre-coated with
1261 Poly-D-Lysine for 30 min at RT. The medium was removed and each well was washed 3x with 100µl
1262 HBSS. The cells were finally analyzed by a fluorescence plate reader (Neo2, BioTek, Bad
1263 Friedrichshall) in HBSS.

1264

1265 **Extracellular oxygen consumption.** HEK293 cells 24h after transfection and hPSCs were harvested
1266 and seeded respectively in 96 multiwell black plate and pre-coated (Geltrex A1413302, Thermo Fisher)
1267 96 multiwell black plate, $5x10^4$ cells for well; after incubation O/N at 37 °C and in 5% CO2, the cell
1268 culture medium was replaced by HBSS and the assay were performed according to the manufacturer
1269 protocols (abcam Extracellular Oxygen Consumption Assay).

1270

1271 **Author Contributions**

1272 PA, FP, IF, ZW, MR, IP, RE, HZ, UZ, MET, JDG, SS, ART, SA conduced primary experiments; MG, CP,
1273 GA, FM, BP, AR contributed to the experimental data; NT and SD contributed tools and reagents. PA, IP, IF,
1274 MR, UZ, AT, KT, VF, FA, FG, MS contributed to experimental design and assisted in writing paper, PA, MJL
1275 and RM conceived and lead the study, and wrote the paper.

1276

1277 **Acknowledgments**

1278 We acknowledge funding from European Union's Horizon2020 Marie Skłodowska-Curie Actions (MSCA)
1279 Program under Grant Agreement 641833 (ONCORNET). We are grateful to Dr. Marco Marcia (EMBL) for
1280 insightful discussion.

1281

1282 **Competing Interests**

1283 The authors declare that they have no conflicts of interest with the contents of this article.

1284

1285 **Data Availability Statement**

1286 Source data are provided with this manuscript.

1287

1288 References
1289

1290 1 Kruse, A. C. *et al.* Muscarinic acetylcholine receptors: novel opportunities for drug
1291 development. *Nat Rev Drug Discov* **13**, 549-560, doi:10.1038/nrd4295 (2014).
1292 2 Fryer, A. D., Christopoulos A. & Nathanson N.M. in *Handb. Exp. Pharmacol.* Vol. 208 1-
1293 499 (2012).
1294 3 Novi, F., Scarselli, M., Corsini, G. U. & Maggio, R. The paired activation of the two
1295 components of the muscarinic M3 receptor dimer is required for induction of ERK1/2
1296 phosphorylation. *J Biol Chem* **279**, 7476-7486, doi:10.1074/jbc.M306818200 (2004).
1297 4 Novi, F., Scarselli, M., Corsini, G. U. & Maggio, R. An unusual form of the association
1298 binding kinetics of N-[3H]methylscopolamine to the split muscarinic M2trunk/M2tail
1299 receptor. *J Pharmacol Exp Ther* **305**, 786-795, doi:10.1124/jpet.102.045393 (2003).
1300 5 Jackson, R. J. & Kaminski, A. Internal initiation of translation in eukaryotes: the picornavirus
1301 paradigm and beyond. *RNA* **1**, 985-1000 (1995).
1302 6 Hellen, C. U. & Sarnow, P. Internal ribosome entry sites in eukaryotic mRNA molecules.
1303 *Genes Dev* **15**, 1593-1612, doi:10.1101/gad.891101 (2001).
1304 7 Calebiro, D., Nikolaev, V. O., Persani, L. & Lohse, M. J. Signaling by internalized G-protein-
1305 coupled receptors. *Trends in Pharmacological Sciences* **31**, 221-228,
1306 doi:https://doi.org/10.1016/j.tips.2010.02.002 (2010).
1307 8 Zhang, X., Bedigian, A. V., Wang, W. & Eggert, U. S. G protein-coupled receptors participate
1308 in cytokinesis. *Cytoskeleton (Hoboken)* **69**, 810-818, doi:10.1002/cm.21055 (2012).
1309 9 Hebert-Chatelain, E. *et al.* A cannabinoid link between mitochondria and memory. *Nature*
1310 **539**, 555-559, doi:10.1038/nature20127 (2016).
1311 10 Suofu, Y. *et al.* Dual role of mitochondria in producing melatonin and driving GPCR signaling
1312 to block cytochrome c release. **114**, E7997-E8006, doi:10.1073/pnas.1705768114 %J
1313 Proceedings of the National Academy of Sciences (2017).
1314 11 Maggio, R. *et al.* Variants of G protein-coupled receptors: a reappraisal of their role in
1315 receptor regulation. *Biochem Soc Trans* **44**, 589-594, doi:10.1042/BST20150239 (2016).
1316 12 Maggio, R., Vogel, Z. & Wess, J. Reconstitution of functional muscarinic receptors by co-
1317 expression of amino- and carboxyl-terminal receptor fragments. *FEBS Lett* **319**, 195-200,
1318 doi:10.1016/0014-5793(93)80066-4 (1993).
1319 13 Park, P. S. & Wells, J. W. Monomers and oligomers of the M2 muscarinic cholinergic receptor
1320 purified from Sf9 cells. *Biochemistry* **42**, 12960-12971, doi:10.1021/bi034491m (2003).
1321 14 Bathe-Peters, M., Gmach, P., Annibale, P. & Lohse, M. J. Linescan microscopy data to extract
1322 diffusion coefficient of a fluorescent species using a commercial confocal microscope. *Data*
1323 *Brief* **29**, 105063, doi:10.1016/j.dib.2019.105063 (2020).
1324 15 Dong, C., Filipeanu, C. M., Duvernay, M. T. & Wu, G. Regulation of G protein-coupled
1325 receptor export trafficking. *Biochim Biophys Acta* **1768**, 853-870,
1326 doi:10.1016/j.bbamem.2006.09.008 (2007).
1327 16 Kamiyama, D. *et al.* Versatile protein tagging in cells with split fluorescent protein. *Nat*
1328 *Commun* **7**, 11046, doi:10.1038/ncomms11046 (2016).
1329 17 Bonfili, L. *et al.* Essential amino acid mixtures drive cancer cells to apoptosis through
1330 proteasome inhibition and autophagy activation. *FEBS J* **284**, 1726-1737,
1331 doi:10.1111/febs.14081 (2017).
1332 18 Thakor, N. & Holcik, M. IRES-mediated translation of cellular messenger RNA operates in
1333 eIF2alpha- independent manner during stress. *Nucleic Acids Res* **40**, 541-552,
1334 doi:10.1093/nar/gkr701 (2012).
1335 19 Holcik, M. & Sonenberg, N. Translational control in stress and apoptosis. *Nat Rev Mol Cell*
1336 *Biol* **6**, 318-327, doi:10.1038/nrm1618 (2005).

1337 20 Newman, L. E., Schiavon, C. & Kahn, R. A. Plasmids for variable expression of proteins
1338 targeted to the mitochondrial matrix or intermembrane space. *Cell Logist* **6**, e1247939,
1339 doi:10.1080/21592799.2016.1247939 (2016).
1340 21 Ishizuka, T., Ozawa, A., Katsuura, M., Nomura, S. & Satoh, Y. Effects of muscarinic
1341 acetylcholine receptor stimulation on the differentiation of mouse induced pluripotent stem
1342 cells into neural progenitor cells. *Clin Exp Pharmacol Physiol* **45**, 1198-1205,
1343 doi:10.1111/1440-1681.12993 (2018).
1344 22 Hoogduijn, M. J., Cheng, A. & Genever, P. G. Functional nicotinic and muscarinic receptors
1345 on mesenchymal stem cells. *Stem Cells Dev* **18**, 103-112, doi:10.1089/scd.2008.0032 (2009).
1346 23 Weinberg, Z. Y. & Puthenveedu, M. A. Regulation of G protein-coupled receptor signaling
1347 by plasma membrane organization and endocytosis. *Traffic* **20**, 121-129,
1348 doi:10.1111/tra.12628 (2019).
1349 24 Jong, Y. I., Harmon, S. K. & O'Malley, K. L. GPCR signalling from within the cell. *Br J*
1350 *Pharmacol* **175**, 4026-4035, doi:10.1111/bph.14023 (2018).
1351 25 Benard, G. *et al.* Mitochondrial CB(1) receptors regulate neuronal energy metabolism. *Nat*
1352 *Neurosci* **15**, 558-564, doi:10.1038/nn.3053 (2012).
1353 26 Lefkimmiatis, K., Leronni, D. & Hofer, A. M. The inner and outer compartments of
1354 mitochondria are sites of distinct cAMP/PKA signaling dynamics. *J Cell Biol* **202**, 453-462,
1355 doi:10.1083/jcb.201303159 (2013).
1356 27 Marti-Solano, M. *et al.* Combinatorial expression of GPCR isoforms affects signalling and
1357 drug responses. *Nature* **587**, 650-656, doi:10.1038/s41586-020-2888-2 (2020).
1358 28 van Heesch, S. *et al.* The Translational Landscape of the Human Heart. *Cell* **178**, 242-260
1359 e229, doi:10.1016/j.cell.2019.05.010 (2019).
1360 29 Pestova, T. V., Shatsky, I. N. & Hellen, C. U. Functional dissection of eukaryotic initiation
1361 factor 4F: the 4A subunit and the central domain of the 4G subunit are sufficient to mediate
1362 internal entry of 43S preinitiation complexes. *Mol Cell Biol* **16**, 6870-6878,
1363 doi:10.1128/mcb.16.12.6870 (1996).
1364 30 Jan, E. & Sarnow, P. Factorless ribosome assembly on the internal ribosome entry site of
1365 cricket paralysis virus. *J Mol Biol* **324**, 889-902, doi:10.1016/s0022-2836(02)01099-9 (2002).
1366 31 Fitzgerald, K. D. & Semler, B. L. Bridging IRES elements in mRNAs to the eukaryotic
1367 translation apparatus. *Biochim Biophys Acta* **1789**, 518-528,
1368 doi:10.1016/j.bbagrm.2009.07.004 (2009).
1369 32 Ingolia, N. T., Hussmann, J. A. & Weissman, J. S. Ribosome Profiling: Global Views of
1370 Translation. *Cold Spring Harb Perspect Biol* **11**, doi:10.1101/cshperspect.a032698 (2019).
1371 33 Zhang, J., Nuebel, E., Daley, G. Q., Koehler, C. M. & Teitell, M. A. Metabolic regulation in
1372 pluripotent stem cells during reprogramming and self-renewal. *Cell Stem Cell* **11**, 589-595,
1373 doi:10.1016/j.stem.2012.10.005 (2012).
1374 34 Guo, C., Sun, L., Chen, X. & Zhang, D. Oxidative stress, mitochondrial damage and
1375 neurodegenerative diseases. *Neural Regen Res* **8**, 2003-2014, doi:10.3969/j.issn.1673-
1376 5374.2013.21.009 (2013).
1377 35 Kritsiligkou, P. *et al.* Unconventional Targeting of a Thiol Peroxidase to the Mitochondrial
1378 Intermembrane Space Facilitates Oxidative Protein Folding. *Cell Rep* **18**, 2729-2741,
1379 doi:10.1016/j.celrep.2017.02.053 (2017).
1380 36 Bonner, T. I., Buckley, N. J., Young, A. C. & Brann, M. R. Identification of a family of
1381 muscarinic acetylcholine receptor genes. *Science* **237**, 527-532, doi:10.1126/science.3037705
1382 (1987).
1383 37 Kozak, M. Constraints on reinitiation of translation in mammals. *Nucleic Acids Res* **29**, 5226-
1384 5232, doi:10.1093/nar/29.24.5226 (2001).
1385 38 Kozak, M. Circumstances and mechanisms of inhibition of translation by secondary structure
1386 in eucaryotic mRNAs. *Mol Cell Biol* **9**, 5134-5142, doi:10.1128/mcb.9.11.5134 (1989).

1387 39 Manders, E. M. M., Verbeek, F. J. & Aten, J. A. Measurement of Colocalization of Objects
1388 in Dual-Color Confocal Images. *J Microsc-Oxford* **169**, 375-382, doi:DOI 10.1111/j.1365-
1389 2818.1993.tb03313.x (1993).
1390 40 Manders, E. M. M., Stap, J., Brakenhoff, G. J., Vandriel, R. & Aten, J. A. Dynamics of 3-
1391 Dimensional Replication Patterns during the S-Phase, Analyzed by Double Labeling of DNA
1392 and Confocal Microscopy. *J Cell Sci* **103**, 857-862 (1992).
1393 41 Richardson, C. D., Ray, G. J., DeWitt, M. A., Curie, G. L. & Corn, J. E. Enhancing homology-
1394 directed genome editing by catalytically active and inactive CRISPR-Cas9 using asymmetric
1395 donor DNA. *Nat Biotechnol* **34**, 339-344, doi:10.1038/nbt.3481 (2016).
1396 42 Vallone, V. F. *et al.* Methods for Automated Single Cell Isolation and Sub-Cloning of Human
1397 Pluripotent Stem Cells. *Curr Protoc Stem Cell Biol* **55**, e123, doi:10.1002/cpsc.123 (2020).
1398 43 Metzler, E., Telugu, N., Diecke, S., Spuler, S. & Escobar, H. Generation of two human
1399 induced pluripotent stem cell lines derived from myoblasts (MDCi014-A) and from peripheral
1400 blood mononuclear cells (MDCi014-B) from the same donor. *Stem Cell Res* **48**, 101998,
1401 doi:10.1016/j.scr.2020.101998 (2020).
1402